THE CONTRACTILE MECHANISM IN CILIA

ROBERT RIKMENSPOEL *and* WALTER G. RUDD

From the Department of Biological Sciences, State University of New York, Albany, New York 12222. Dr. Rudd's present address is the Department of Computer Sciences, Louisiana State University, Baton Rouge, Louisiana 70803.

ABSTRACT A detailed analysis is made of the motion and the forces in the cilium of *Sabellaria* over the complete cycle. The results indicate that the stiffness of the cilium is directly related to the moments produced by the internal contractile elements. A sliding filament model is developed to generate the complete cycle of motion. The activation of the force-producing elements, the peripheral fibers, occurs over their entire length at once during the effective stroke. In the recovery stroke the sliding of peripheral fibers relative to each other produces activation. The peripheral fibers contribute to the stiffness of the cilium in the sliding filament model only when they are not free to slide because of cross-linkage. The model describes successfully the motion of a variety of types of cilia.

INTRODUCTION

In recent years much attention has been focused on the contractile events in cilia and flagella (for a review, see Miller, 1968). The same basic structure of nine peripheral longitudinal fibers, running the entire length of both these organelles, has been found with the electron microscope (see Fawcett, 1966). A pair of fibers runs along the central axis of flagella and cilia in practically all species.

Each of the nine peripheral fibers consists of a double tubule. At regular intervals of 170 Å along the length of each peripheral fiber a pair of "arms" extends in the direction of the adjacent fiber. Gibbons (1963) has shown that these arms, termed "dynein," have ATPase activity. Dynein is therefore generally assumed to be the force-producing molecule in cilia and flagella.

Satir (1965, 1968) has proposed that the forces in cilia and flagella are produced by a sliding filament mechanism, in analogy to striated muscle. The dyneins are assumed to form cross bridges between adjacent peripheral fibers. The occurrence of such a mechanism has recently conclusively been shown by Summers and Gibbons (1971) to occur in these structures.

The function of the central fibers remains a mystery until now. One apparent question is how the contractility, that is the formation of cross bridges, is coordinated. To produce the observed motion in cilia and flagella, forces have to be developed in the right sequence in time and at the right location. Where the same

structure and chemistry is found in both these organelles, one expects the same basic principles to apply to the coordination of contractility in both.

Most work has been done on flagella. Because flagellar motion appears harmonic in time, periodic solutions for theoretical models are allowed, which simplifies the analysis. Several models have been developed (Brokaw, 1972 *a*; Lubliner and Blum, 1971, 1972; Rikmenspoel, 1971) which will be related in the Discussion of this paper.

For cilia detailed observations have become available recently (Sleigh, 1968). These observations show a large variety in motion of cilia of different species.

In this paper a detailed analysis is carried out of the motion and the forces in the cilium of *Sabellaria*. The results are used to develop a model for the coordination of the force-producing events in it. The model is then tested for its ability to describe other types of ciliary motion. A comparison with the models for flagella is also made. A preliminary publication of some of the results of this paper has been made recently (Rikmenspoel and Rudd, 1972).

LIST OF SYMBOLS

a	Radius of cylindrical cilium.
b	Exponent.
c	Radius of cylindrical disk.
D	Density of dynein molecules per centimeter in axoneme.
D_0	Density of dyneins per centimeter at base of cilium.
d	Thickness of a plate.
$\mathbf{F}$	Viscous drag force.
$f, f(\xi, t)$	Fraction of dyneins activated at time t, location ξ.
$f_{eff}, f_{eff}(t)$	Fraction of dyneins activated for effective stroke.
$f_{rec}, f_{rec}(\xi, t)$	Fraction of dyneins activated for recovery stroke.
$IE, IE(s)$	Stiffness of cilium, at location s.
IE_{fibers}	Stiffness contribution of peripheral fibers to total stiffness.
IE_{mat}	Stiffness contribution of matrix and membrane material.
$IE_{rec}(s)$	Stiffness contribution of peripheral fibers to total stiffness during recovery stroke.
$ie, ie_{mat}, ie_{fibers}$	Same as capitalized symbols, but valid for single axoneme.
K	Viscous drag of a disk.
k	Drag coefficient of cilium per unit length.
k_N	Viscous drag coefficient for normal motion.
k_T	Viscous drag coefficient for tangential motion.
k_{visc}	Drag coefficient per unit length due to viscous forces only.
L	Length of a cilium.
M	Symbolic expression for viscous moment.
M_{act}	Active moment due to contractile forces.
M_{eff}	Active moment for effective stroke.
M_{el}	Elastic bending moment.
M_{rec}	Active moment for recovery stroke.
M_{visc}	Moment due to viscous resistance of cilium.
m_e	Active moment produced by one dynein molecule.

$m(t)$	Active moment at base ($s = 0$), at time t.
N	Number of component axonemes of a cilium.
n	Number of equations in iteration procedure.
p	Exponent.
R	The Reynolds number.
$\mathbf{r}_{s\xi}$	Straight distance between locations s and ξ on cilium.
r_x, r_y	Projection of $\mathbf{r}_{s\xi}$ on x and y axis, respectively.
s	Location on cilium, arc length to base.
s_b	Point of maximum curvature during recovery stroke.
Δs	Length interval, $\Delta s = L/n$.
δs	Length over which stiffness due to peripheral fibers is averaged.
t	Time.
t_{act}	Time during which activation signal for effective stroke is present.
Δt	Time length of iteration step.
t_0	Beginning of recovery stroke.
V	Characteristic velocity, to be used in the Reynolds number.
$\mathbf{V}_\xi$	Velocity of displacement of segment $d\xi$ of cilium.
V_T, T_N	Tangential and normal component of V_ξ
V_T^x, V_T^y	Projection of V_T on x and y axis, respectively.
V_N^x, V_N^y	Projection of V_N on x and y axis, respectively.
v	Velocity at which the bend during the recovery stroke travels over cilium.
x	Cartesian coordinate normal to cell surface.
y	Cartesian coordinate tangential to cell surface.
z	Dimensionless arc length coordinate: $z = s/L$.
α	Dimensionless parameter, to account for difference in drag coefficient in effective and recovery stroke.
Δ	Length of bend section during recovery stroke.
η	Viscosity of medium.
θ, $\theta(s)$	Angle with x axis, at location s.
θ_0	Angle with x axis of cilium at point of implantation.
θ_i	Value of θ at end of ith length interval.
θ_i^t, $\theta_i^{t+\Delta t}$	Value of θ_i at time t and $t + \Delta t$, respectively.
λ	Wavelength.
μm	Micron.
ν	Kinematic viscosity.
ξ	Running coordinate, in arc length.
ρ	Radius of curvature.
$\sigma(s)$, $\sigma(\xi)$	Density of dynein molecules as function of location, normalized to $\sigma(0) = 1$.
τ_{eff}	Decay time of activation in effective stroke.
τ_{rec}	Decay time of dynein attachment in recovery stroke.
χ	Running coordinate, in arc length.
ζ	Running coordinate, in arc length.

EXPERIMENTAL DATA

A full cycle of the motion of the cilium of *Sabellaria* is shown in Fig. 1, taken from Rikmenspoel and Sleigh (1970). The effective stroke of the cilium (0–24 ms) is shown at 3-ms intervals, the recovery stroke (24–60 ms) at 6-ms intervals.

The cycle shown in Fig. 1 had been chosen as being representative for the motion

of this type of cilium. The tracing of the positions of the cilium from the cinemicrographs was done with an accuracy equivalent to a fraction of a micron in the preparation. At the point of implantation of the cilium the image on the cinemicrographs was less clear due to the optical effects of the cell surface. The angle of implantation

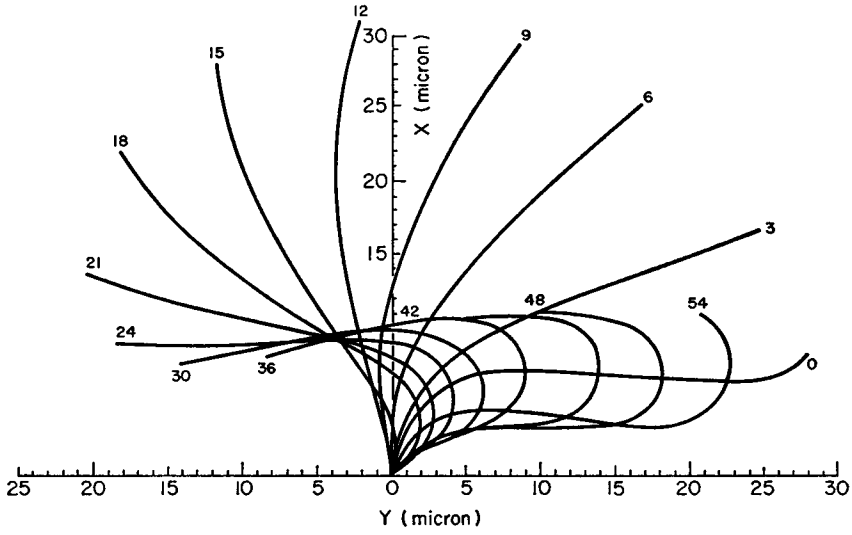

FIGURE 1 Complete cycle of the cilium on the dorsal gill of *Sabellaria*. The effective stroke is shown at 3-ms intervals, the recovery stroke at 6-ms intervals (reprinted from *J. Theor. Biol.* **28**:81).

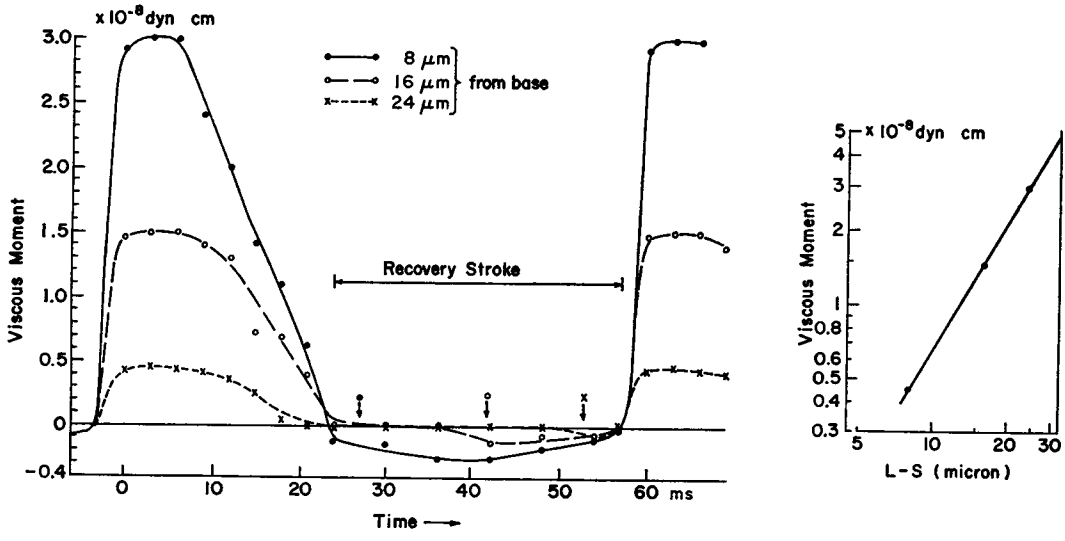

FIGURE 2 (A) Viscous moments on the cilium in Fig. 1 at three locations on the cilium, during the cycle (reprinted from *J. Theor. Biol.* **28**:81). (B) Viscous moment in the period 3–9 ms plotted as a function of location on the cilium.

could therefore not be read from the films to an accuracy of better than several degrees.

The *Sabellaria* cilium is a compound of 25–30 cilia, each having a 9 + 2 structure. No structures have been found that bind the component cilia to each other (Sleigh, 1962). This phenomenon of many components moving together as a unit, without any apparent structure holding the assembly together, is a general property of compound cilia (Sleigh, 1962).

In an earlier paper (Rikmenspoel and Sleigh, 1970) small amplitude elastic theory (under neglect of active, contractile forces) was applied to this compound cilium. From this analysis an estimate of the stiffness during the recovery stroke of $(2 \pm 1) \times 10^{-13}$ dyn cm^2 was reported.

The moments due to the viscous resistance of the cilium were calculated by Rikmenspoel and Sleigh (1970). Fig. 2 shows the results. The data presented in Fig. 1 and Fig. 2 form the basis for the analysis applied to the *Sabellaria* cilium in this paper. More or less schematic descriptions of cilia of *Paramecium*, *Stentor*, and *Jorunna*, from Sleigh (1962, 1968) and a detailed description of the "comb plate" compound cilium of *Pleurobrachia* (Sleigh and Jarman, 1973) are shown in Figs. 20–23, in the section Other Types of Ciliary Motion.

EQUATION OF MOTION

In a cilium with active internal force-producing elements the moments due to the elasticity M_{el} and due to the contractility M_{act} are at any time balanced by the viscous moment M_{visc}:

$$M_{el} + M_{act} = M_{visc}. \tag{1}$$

For cilia it is essential, as Fig. 1 shows, to use large amplitude algebra in evaluating the terms in Eq. 1. Fig. 3 illustrates the coordinate system used, in which s is the independent variable, and θ the dependent one. Normal cartesian coordinates are found from $x = \int_0^s \cos\theta(s)\,ds$ and $y = \int_0^s \sin\theta(s)\,ds$. The sign conventions which we used (positive = counterclockwise) are shown in Fig. 3.

The exact expression for the elastic moment becomes

$$M_{el} = IE\frac{1}{\rho} = IE\frac{\partial\theta}{\partial s}, \tag{2}$$

where IE is the stiffness of the cilium (E is the elasticity modulus of the material, I is the second-order moment of the cross section) and ρ is the radius of curvature of the cilium at s.

To the viscous moment at s, all segments of the cilium distal to s contribute. A segment $d\xi$, located at ξ moving with velocity V_ξ, has a drag force $\mathbf{F} = -k\,\mathbf{V}_\xi\,d\xi$, where k is the drag coefficient. With a lever $\mathbf{r}_{s\xi}$ (see Fig. 3) the moment $dM(\xi)$ due to segment $d\xi$ is:

$$dM(\xi) = -k(\mathbf{V}_\xi \times \mathbf{r}_{s\xi})\,d\xi.$$

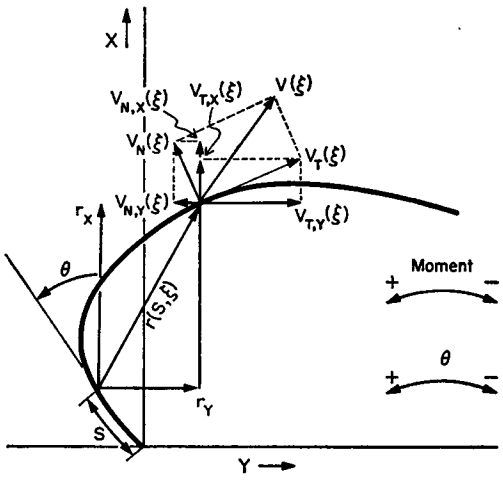

FIGURE 3 Coordinate system used in evaluating the terms of the equation of motion.

Since the drag coefficient for tangential motion is one-half of that for motion normal to the axis (Hancock, 1955), it is necessary to decompose $\mathbf{V}_\xi$ and $\mathbf{r}_{s\xi}$ as shown in Fig. 3 and

$$dM_{visc}(\xi) = -\{(k_T V_T^X + k_N V_N^X) r_Y + (k_T V_T^Y + k_N V_N^Y) r_x\}\, d\xi,$$

where $k_N = k$ and $k_T = \frac{1}{2}k$.

With $r_x = \int_s^\xi \cos\theta(\zeta)\, d\zeta$, $V_T^X = \cos\theta(\xi) \int_0^\xi -\sin\theta(x)[\partial\theta(x)/\partial t]\, dx$, $V_N^X = -\sin\theta(\xi) \int_0^\xi -\sin\theta(x)\ [\partial\theta(x)/\partial t]\, dx$ and analogous expressions for r_Y, V_T^Y, and V_N^Y, the complete expression for $dM_{visc}(\xi)$ becomes:

$$\begin{aligned} dM_{visc}(\xi) = {} & -k[\tfrac{1}{2}\sin\theta(\xi)\cos\theta(\xi) \int_0^\xi \sin\theta(\chi) \frac{\partial\theta(\chi)}{\partial t}\, d\chi \int_0^\xi \cos\theta(\zeta)\, d\zeta \\ & + \{\cos^2\theta(\xi) + \tfrac{1}{2}\sin^2\theta(\xi)\} \int_0^\xi \cos\theta(\chi) \frac{\partial\theta(\chi)}{\partial t}\, d\chi \int_s^\xi \cos\theta(\zeta)\, d\zeta \\ & + \{\sin^2\theta(\xi) + \tfrac{1}{2}\cos^2\theta(\xi)\} \int_0^\xi \sin\theta(\chi) \frac{\partial\theta(\chi)}{\partial t}\, d\chi \int_s^\xi \sin\theta(\zeta)\, d\zeta \\ & + \tfrac{1}{2}\sin\theta(\xi)\cos\theta(\xi) \int_0^\xi \cos\theta(\chi) \frac{\partial\theta(\chi)}{\partial t}\, d\chi \int_s^\xi \sin\theta(\zeta)\, d\zeta]\, d\xi. \end{aligned} \tag{3}$$

The total viscous moment at s is

$$M_{visc}(s) = \int_s^L dM_{visc}(\xi), \tag{4}$$

where L is the length of the cilium. The complicated expression for M_{visc} given in

Eqs. 3 and 4 can be written symbolically as

$$M_{\text{visc}} = kM(\partial\theta/\partial t, \cos\theta, \sin\theta). \tag{5}$$

The internal, active moment $M_{\text{act}}(s, t)$ produced by the contractile elements we shall leave unspecified for the time being. The complete equation of motion thus becomes:

$$IE(\partial\theta/\partial s) + M_{\text{act}}(s, t) = kM(\partial\theta/\partial t, \cos\theta, \sin\theta). \tag{6}$$

Eq. 6 can be easily iterated in time by converting it into a system of linear equations. If we divide the length of the cilium into n segments Δs, with $L = n\Delta s$, the position of the cilium at time t is defined by θ_i^t $(i = 0, 1, 2, \cdots, n)$. For the elastic term at i we can write for the iteration step from t to $t + \Delta t$:

$$IE\frac{\partial\theta_i^{t+\Delta t}}{\partial s} = IE(\theta_{i+1}^{t+\Delta t} - \theta_{i-1}^{t+\Delta t})/2\Delta s \quad (i = 1, 2, \cdots, n-1). \tag{7}$$

The symbolic expression for the viscous moment at i, M_i, becomes

$$M_i = M_i[(\theta_j^{t+\Delta t} - \theta_j^t)/\Delta t, \cos\theta_j^t, \sin\theta_j^t],$$
$$(j = 0, 1, 2, \cdots, n), (i = 1, 2, \cdots, n-1). \tag{8}$$

Trapezoidal rule was used to evaluate the integrals of Eqs. 3 and 4.

For an iteration in time the values for all θ's at time t are known. Substitution of Eqs. 7 and 8 into Eq. 6 yields, after sorting out the terms, $n - 1$ linear equations in $\theta_i^{t+\Delta t}$ $(i = 1, 2, \cdots, n)$.

The viscous moment vanishes at the free end according to Eq. 4. The active contractile moment also vanishes at the free end, since the contractile peripheral fibers vanish a few microns before reaching the tip of the cilium (Satir, 1965). Therefore $\partial\theta/\partial s = 0$ $(s = L)$. With the aid of $(\partial\theta/\partial s)(s = L) = (\partial\theta/\partial s)(s = L - \Delta s) + (\partial^2\theta/\partial s^2)\Delta s$ $(s = L - \Delta s)$, we find as the nth equation:

$$3\theta_n^{t+\Delta t} - 4\theta_{n-1}^{t+\Delta t} + \theta_{n-2}^{t+\Delta t} = 0. \tag{9}$$

Eqs. 7 and 9 both refer to the elastic term in Eq. 6. It is essential to write the (unknown) value of θ at time $t + \Delta t$ in these equations, not the (known) value at t. In this latter case the iteration procedure quickly diverges. This can be understood as using the "bending resistance" of the cilium, instead of the "bending moment."

At the point of attachment of the cilium $(i = 0)$ the values of θ_0 were measured from Fig. 1, and inserted as known values in the set of simultaneous equations. This corresponds to treating the cilium as being clamped at the base.

The technique described above was programmed for a Univac 1108 computer.

When using 16 equations ($n = 16$) the time required for one iteration step was about 1 s. With $n = 32$ one iteration took approximately 7 s. The iteration procedure converged for an indefinite number of iterations. The motion of the model cilium was found to be independent of the number of segments used, or the length Δt of the time interval, within rather large limits. An iteration technique somewhat similar to the one described above was used by Brokaw (1972 *a*) for an analysis of flagellar motion.

ITERATION IN TIME FOR *SABELLARIA*

The *Sabellaria* cilium shown in Fig. 1 has a length $L = 32$ μm. The iteration procedure was performed with $n = 16$, giving a length interval $\Delta s = 2$ μm. As time interval we chose $\Delta t = 1$ ms. This means that everywhere, except at the tip of the cilium at the beginning of the cycle, the motion per iteration is less than Δs.

The value of θ_0 was read from Fig. 1 and plotted vs. time. The curve drawn through the plotted points was approximated as $\theta_0 = 0$ ($t = 0$–12 ms), $\theta_0 = -0.5$ $[1 - \cos\{(t - 0.024)/200\}]$ ($t = 12$–24 ms), $\theta_0 = -0.5$ ($t = 25$–50 ms), $\theta_0 = -0.5 + 60$ $(t - 0.050)$ ($t = 51$–54 ms).

During the recovery stroke (24–60 ms) the *Sabellaria* cilium has a wavelike shape. In that case the viscous drag coefficient for normal motion is given by Gray and Hancock (1955) as

$$k = -\frac{4\pi\eta}{0.5 + \ln(a/2\lambda)}. \qquad (10)$$

With $\eta = 1$ cP, the radius of the cross section of the compound cilium $a = 0.5$ μm (Sleigh, 1962) and taking for λ twice the length of the bent section ($\lambda \approx 12$ μm), the value for k becomes $k = 0.037$ dyn cm^{-2} s. The same value for k was used in the earlier paper on the *Sabellaria* cilium.

During the effective stroke the cilium may more properly be considered as a rod moving perpendicular to its axis. For that case, the drag coefficient for normal motion is given by (Lamb, 1952)

$$k = \frac{4\pi\eta}{0.5 - \gamma - \ln(Va/4\nu)}, \qquad (11)$$

where $\gamma = 0.577$ is the constant of Euler, V is the velocity of the rod, and ν is the kinematic viscosity of the medium. If we take as characteristic value for V the value halfway along the cilium during the active stroke, then $V = 0.17$ cm/s. With $\nu = 1$ cSt, the value derived from Eq. 11 is $k = 0.015$ dyn cm^{-2} s.

In the effective stroke the cilium is bent, however. The motion is also not perpendicular to its axis, but angular. No hydrodynamic theory has been developed which describes this type of motion. Consequently we do not really know what the

drag coefficient during the effective stroke is, except that from Eq. 11 we may expect it to be lower than during the recovery phase.

In the absence of a more precise knowledge of the drag coefficient we have carried out the analysis with a fixed drag coefficient $k = 0.037$ dyn cm^{-2} s. In Eq. 6 we observe that k acts as a proportionality constant for all of the moments. With the fixed value of $k = 0.037$ dyn cm^{-2} s the values for the stiffness and the active moments to be derived for the effective stroke may therefore all be systematically too high. We shall come back to this question in the section Contractile Model.

Effective Stroke (0–24 ms)

It can be seen in Fig. 2 A that during the effective stroke the viscous moment varies in time in the same way at different points of the cilium. The elastic moment should be small during most of the effective stroke (3–15 ms), since the cilium is only little curved. The active moment should, therefore, not be much different from the viscous one (compare Eq. 6), and it is logical to write

$$M_{act} = m(t)(1-s/L)^p. \qquad (12)$$

From Fig. 2 B we have taken $p = 1.75$.

For the iteration procedure we have taken as starting position the position of the cilium at $t = 0$. When a moment of the form of Eq. 12 is applied to the cilium the first calculation showed that the movement of the tip of the cilium is mainly determined by the magnitude of the moment, and that the shape acquired by the cilium is mainly dependent on the stiffness.

Fig. 1 shows that for $t = 3$–12 ms, the velocity of the tip of the cilium is approximately constant at 3.4 μm/ms. This tip velocity can be reproduced in our computed model with a value for the moment at the base, $m(t)$ of Eq. 12, of approximately 4×10^{-8} dyn cm.

At values of the stiffness IE less than 10^{-12} dyn cm^2 no meaningful results were obtained as the matrix of the set of linear equations proved to be too near singular. With $IE > 6 \times 10^{-12}$ dyn cm^2 the model cilium was clearly showing too little curvature.

With these initial observations of the separate effects of the magnitude of the moment and of the stiffness and with the above determinations of the approximate range of $m(t)$ and IE, further quantitation was possible. In all calculations reported below we have let the magnitude of the active moment in the period 0–3 ms rise proportionally with time from 0 to its constant value for 3–9 ms (compare Fig. 7). In this initial period of the effective stroke application of the full active moment resulted in a velocity of the tip of the cilium at 0–3 ms which was about twice too high. Apparently the active moment requires a few milliseconds to develop fully. Because of this effect we have not used the 3 ms position to evaluate the active moment, but the positions at 6 and 9 ms.

Fig. 4 shows computed positions of the cilium at 6 ms at various values of the active moment. It can be seen in Fig. 4 that the radius of curvature ρ at the place of maximal bending of the cilium is only little dependent on the active moment. At a value of $m(t) = 3.8 \times 10^{-8}$ dyn cm the best representation of the 6, 9, and 12 ms positions is obtained (Fig. 9). This value is about 20% lower than that obtained from extrapolation of the data shown in Fig. 2 B to $s = 0$. In view of the crude way in which Fig. 2 had been calculated, we can consider the two values to be satisfactorily close.

To determine IE we have used the value of the maximal curvature on the computed cilium. Fig. 5 illustrates that with $m(t) = 3.8 \times 10^{-8}$ dyn cm, the position of the tip of the cilium at 6 ms varies by only a few microns if the stiffness is varied by a factor of 5. The minimal radius of curvature ρ occurring on the computed cilium at 3, 6, and 9 ms is shown in Fig. 6 as a function of the stiffness IE. The values for ρ at 3, 6, and 9 ms measured from Fig. 1 are shown as the open circles in Fig. 6. At 3 ms the computed value of ρ depends little on IE; probably the "memory" of the sharp bend at $t = 0$ is still dominant at 3 ms. We have therefore not included ρ at 3 ms in the determination of IE. The values of ρ at 6 and 9 ms give a stiffness $IE = 3 \times 10^{-12}$ dyn cm^2 (rounded off because of the uncertainty in the drag coefficient).

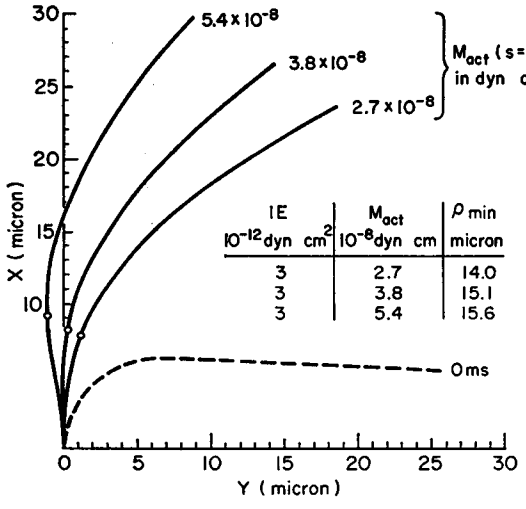

FIGURE 4

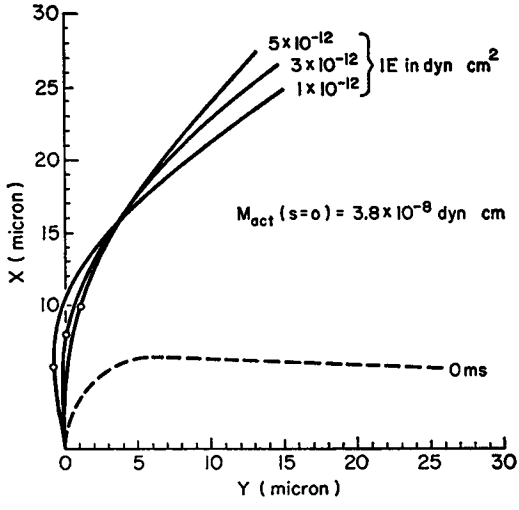

FIGURE 5

FIGURE 4 Computed positions at 6 ms with a constant stiffness of 3×10^{-12} dyn cm^2 for three different values of the active moment. The insert table shows the radius of curvature (ρ_{min}) at the point of maximal bending (indicated by the open circles) for the three different values of the active moment.

FIGURE 5 Computed positions of the cilium at 6 ms for three different values of the stiffness IE. The magnitude of the active moment at the base was 3.8×10^{-8} dyn cm in all three cases. The circles indicate the location on the computed positions where the curvature was maximal.

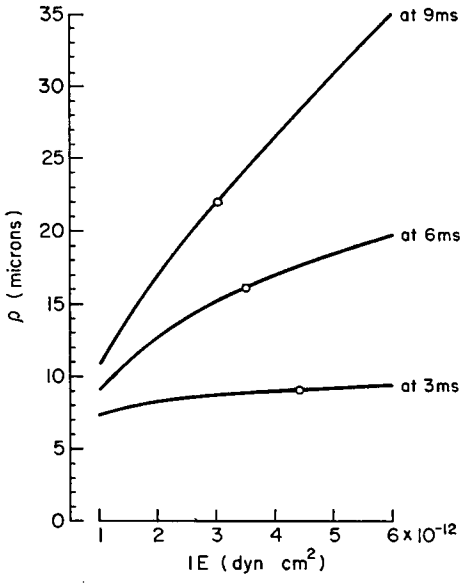

FIGURE 6

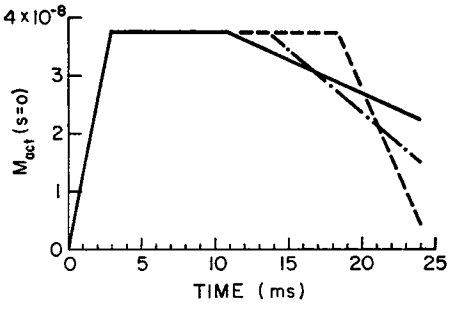

FIGURE 7

FIGURE 6 Radius of curvature ρ, at the place of maximal curvature, of the computed positions at 3, 6, and 9 ms as a function of the stiffness IE. The active moment at the base was 3.8×10^{-8} dyn cm in all cases. The circles indicate the value for ρ measured from the data in Fig. 1.

FIGURE 7 Variation in time of the magnitude of the active moment at the base. The area under the three different curves in the period 0–24 ms is the same.

When the iteration is continued beyond 9 ms, with the values $m(t) = 3.8 \times 10^{-8}$ dyn cm and $IE = 3 \times 10^{-12}$ dyn cm^2, the tip of the cilium moves too fast in the latter parts of the effective stroke (20–24 ms). Obviously the active moment is reduced in that period, as suggested already in Fig. 2. We have found, however, that to attain a position at 24 ms in which the distal part of the cilium is parallel to the y axis, it is not important how $m(t)$ varies with time as long as $\int_0^{24} m(t)\,dt$ has the correct value. This is illustrated in Fig. 7, where the three different variations with time of $m(t)$ all give a position at 24 ms which is practically identical within plotting accuracy.

The dotted line in Fig. 8 shows the computed position at 24 ms, obtained with $m(t)$ varying as in Fig. 7. If we compare the computed position at 24 ms in Fig. 8 with the observed one in Fig. 1, we see first that the curvature in the proximal part of the computed position is too small. This indicates that the stiffness of the model cilium in the latter part of the effective stroke was too big. Indeed, we have found that the correct value of the curvature at 24 ms can be obtained if the stiffness for $t > 12$ ms is gradually reduced. The amount of reduction is not critical. If the stiffness for $t > 12$ ms is reduced linearly with time, the correct curvature can be obtained when the stiffness at 24 ms has been brought down to (0.4–0.15) times the original value

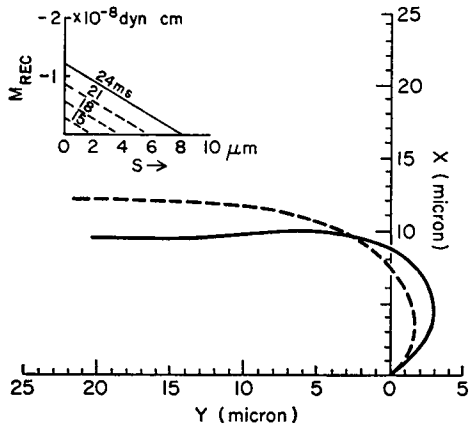

FIGURE 8 Computed positions at 24 ms. The dashed line was obtained with a constant stiffness at all times of 3×10^{-12} dyn cm². The continuous line was obtained with a reduced stiffness in the latter part of the effective stroke (15–24 ms) and an amount of recovery active moment present as indicated in the inset (see text).

of 3×10^{-12} dyn cm^2. This is compatible, for the dashed and the dashed-dotted lines in Fig. 7, with the stiffness of the model cilium being taken proportional to $m(t)$.

Secondly, we observe in Fig. 8 that the proximal part of the model does not move out to the right as far as it should according to Fig. 1. This implies that extra active moment of negative sign (see Fig. 3) is present in the proximal part. Apparently the recovery stroke has started before the termination of the effective stroke. This overlap of the two phases has been noted before by Sleigh (1968). It is also indicated by the fact that the angle of implantation (θ_0) of the observed cilium starts to change at 12 ms, well before the end of the effective stroke.

If a small amount of negative active moment (moments of negative sign we will call M_{rec}) is added as shown in the top of Fig. 8, the computed movement to the right is close to the observed one. The solid line in Fig. 8 gives the computed position at 24 ms, obtained with $m(t)$ varying as the dash-dot curve in Fig. 7, with the stiffness varying proportional to $m(t)$, and with M_{rec} as shown in Fig. 8.

The total effective stroke at 3-ms intervals, computed as related in the preceding paragraph, is given in Fig. 9. Comparing Figs. 9 and 1 we see that the general appearance of the observed effective stroke is rather well reproduced in the model. The "spacing" of the consecutive positions, as indicated by the tip of the cilium, is more regular in the model. At 24 ms, the movement to the right of the proximal part is about 1 μm to little. Both these deviations are undoubtedly caused by the too simple approximations of M_{act} and M_{rec}.

We also see, however, that from 12 to 24 ms the observed cilium has a clear curvature near the tip, which is absent for the model. This indicates that the stiffness in the distal part is reduced, and that our assumption of a constant IE along the cilium

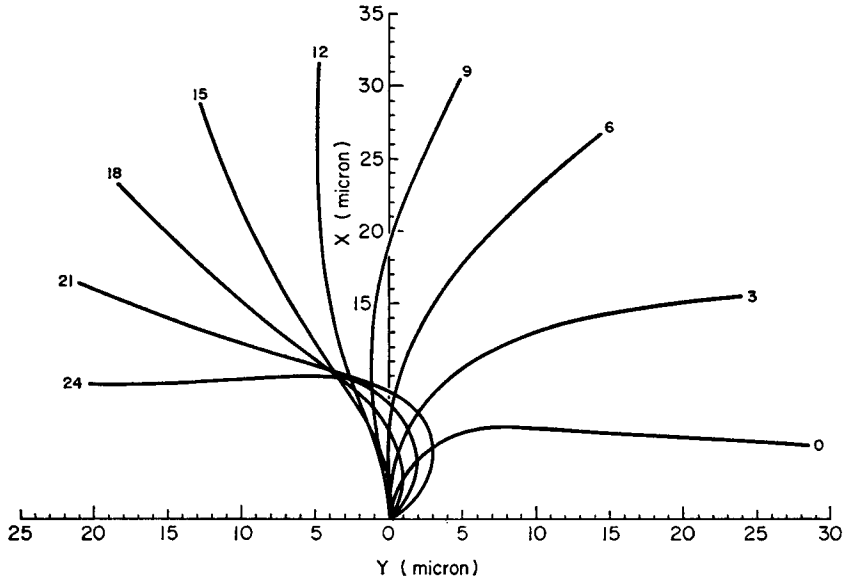

FIGURE 9 Computed effective stroke at 3-ms intervals. The variation of the active moment and stiffness with time is explained in the text.

was an oversimplification. It should be noted that a stiffness which reduces towards the tip of the cilium (where the movements are smaller) ties in well with our findings of the variation of the stiffness (and moments) with time. In the section Contractile Model for Cilia we shall indeed see that a variation of the stiffness along the cilium can give improvement of the representation of the distal part.

We have tried to see whether a different value of the constant p of Eq. 12, which has been held constant at $p = 1.75$ could give the same or a better representation of the active stroke. Our findings were that when p is significantly lower than 1.75, the distal part of the cilium bends over in the "forward" direction, especially in the latter part of effective stroke, which is contrary to the observation. When $p > 1.75$ the distal part of the cilium in the early phase (0–9 ms) lags, and a pronounced inflection develops in the cilium in the latter part of the effective stroke (15–21 ms). A detailed presentation of these results does not seem to be warranted. It appears, however, that our choice of $p = 1.75$ gives the best overall results.

Recovery Stroke (24–54 ms)

As Fig. 2 indicates, the viscous moment during the recovery stroke (24–54 ms) changes differently with time at different locations on the flagellum. We cannot assume that the elastic moments in the cilium are small compared with the viscous one, because a strong curvature occurs on the cilium. For these reasons we are not justified in taking the viscous moment of Fig. 2 as a guiding value for the active moment, and the separation of the time and space dependency of the active

moment, as done in Eq. 12 for the effective stroke, is also not possible for the recovery phase.

The only conclusion we can draw from Fig. 2 is that the magnitude of the active moments at 24–54 ms is below 10^{-8} dyn cm. A search for the active moments and the stiffness that will produce a motion as seen during the recovery stroke is largely a question of trial and error. We describe below the main results of our calculations. Most of the trials giving negative results will be mentioned only briefly.

Whenever negative active moment is applied, during the recovery phase, beyond the sharply bent section of the cilium, it is found that the distal part shows motion upward, perpendicular to the ciliary axis. Fig. 1 shows quite clearly that the distal part of the cilium has in fact only axial motion for $t > 30$ ms. We can conclude therefore that beyond the bent portion in the recovery stroke no active moment is developed.

During the recovery stroke the radius of curvature in the bent portion of the cilium is practically constant at 4 μm. If the stiffness of the model cilium during the recovery stroke is taken to be greater than 3×10^{-13} dyn cm^2, the radius of curvature is at no time smaller than 5 μm. When the stiffness is taken to be less than 10^{-13} dyn cm^2, no meaningful results are obtained.

When we restrict ourselves during the recovery stroke to a stiffness $IE_{rec} = (2.5 \pm 1.5) \times 10^{-13}$ dyn cm^2, and an active moment M_{rec} which vanishes distal to the point at which the observed cilium of Fig. 1 has maximal bending, the iteration procedure leads to positions that have resemblance to the actual ones. The shape of the computed recovery stroke proves to be very sensitive to the form of M_{rec} used. This is illustrated in Fig. 10. The active moments used in Fig. 10 were $M_{rec} =$

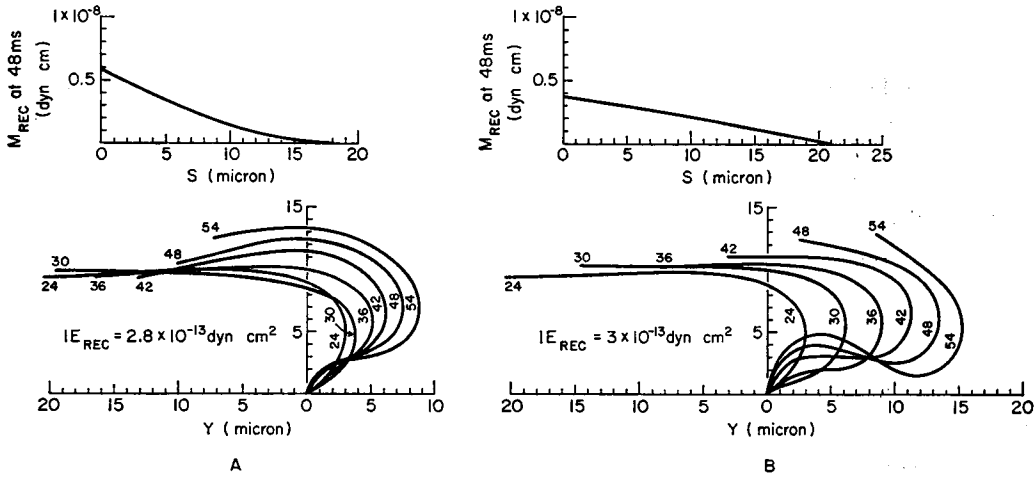

FIGURE 10 Computed recovery strokes for two different shapes of the active moment. The stiffness was constant along the cilium in these computations.

$m(1 - s/s_b)^b$, where s_b is the point of maximal curvature on the real cilium of Fig. 1; $b = 1.75$ in Fig. 10 A, and $b = 0.75$ in Fig. 10 B.

The shape of the two computed recovery strokes in Fig. 10 is quite different. One common property is, however, that the position of the bend travels much slower than in the real cilium. At 54 ms s_b, the "end point" of M_{rec}, is at 4 μm from the tip, much ahead of the bend in the models. After extensive trials we have concluded that no shape of M_{rec} will give a recovery stroke which rolls off at the proper velocity.

However, when the stiffness of the cilium proximal to s_b is taken to be three to five times the stiffness of the part distal to s_b, recovery strokes can be computed which do roll off with the right velocity. The shape of the model cilium during the recovery stroke, with IE_{rec} varying along s, remains very sensitive to the form of the active M_{rec}. It is not much dependent, however, on the factor by which the stiffness proximally to s_b has been increased.

Once this observation had been made it was rather simple, though tedious, work to find by iteration the moments and stiffness which gave the best approximation for the recovery stroke. A constant value at all times for IE_{rec} distally to s_b of 1.8×10^{-13} dyn cm^2 was used. This gave approximately the correct value ($\rho \approx 4$ μm) for the maximal curvature. The form of M_{rec} was approximated by straight segments.

Fig. 11 shows the best result obtained in the iteration procedure. The values by which IE_{rec} was to be increased proximally for optimal results are listed in Table I. The extensive trials done with variations of the form of M_{rec} lead us to believe that

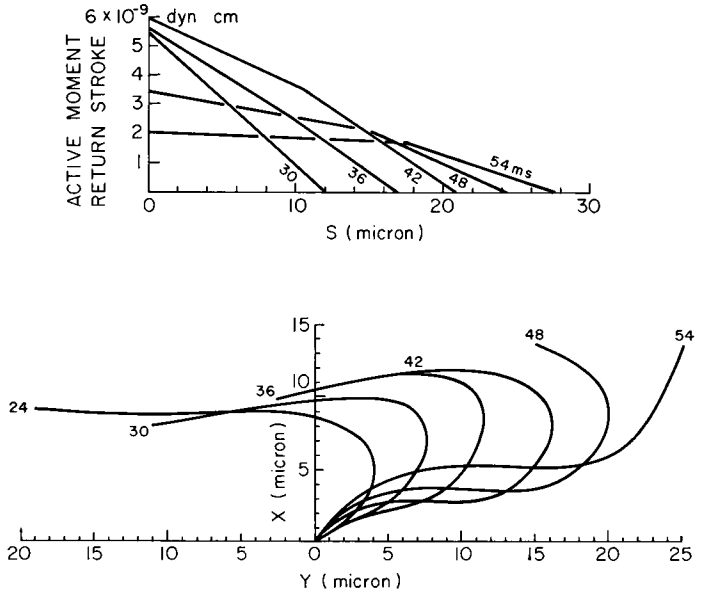

FIGURE 11 Iterated recovery stroke. The stiffness of the part of the cilium proximal to the point of maximal bending was taken to be 3–3.5 times that of the distal portion (Table I). The active moments at various times are shown in the top part of the figure.

TABLE I

FACTOR BY WHICH STIFFNESS PROXIMAL TO BEND WAS INCREASED, DURING ITERATION OF RECOVERY STROKE

Time, *ms*	24–30	30–36	36–42	42–48	48–54
Ratio $\frac{IE_{\text{proximal}}}{IE_{\text{distal}}}$	3.0	3.0	3.5	3.5	3.0

only moments which closely resemble those shown in the top part of Fig. 11 will lead to the correct recovery stroke.

Close comparison of the computed recovery stroke of Fig. 11 and the data of Fig. 1 shows that in the bent portion of the cilium the curvature in Fig. 1 is constant over the bend, whereas in Fig. 11 the proximal part of the curve has less curvature than the distal part. This reflects the abrupt change in stiffness which we used in the calculations. In a real cilium the change in stiffness is therefore probably more gradual.

CONTRACTILE MODEL FOR CILIARY MOTION

In this section we want to develop a model for the contractile coordination in cilia which can in a simple way generate the complete cycle of motion. Summarizing the results of the iteration procedure of the preceding section, we can say that the model should comprise: (*a*) a stiffness of the cilium which is related to the amount of active moment, (*b*) an active moment during the effective stroke which is developed in phase over the entire length of the cilium, (*c*) activation of the contractile elements during the recovery stroke which is initiated by the bend in the cilium, and (*d*) an explanation for the different shapes of the active moments developed during the effective and the recovery stroke.

As mentioned in the Introduction, each of the approximately 30 components of which the compound *Sabellaria* cilium is made up, shows in the electron microscope nine peripheral doublet fibers with a pair of single fibers in the center. Fig. 12 A shows a cross section (after Afzelius, 1959) of this structure. Summers and Gibbons (1971) have shown experimentally the occurrence of a "sliding filament" mechanism between adjacent peripheral fibers. This can be visualized as in Fig. 12 B, where the dyneins form cross bridges between adjacent fibers. The important property of a sliding filament mechanism is that the force-producing elements (myosin in muscle, dyneins in cilia or flagella) are arranged in parallel. The forces produced by the dyneins (or myosins) are summed along the fiber. It has been reported before (Rikmenspoel, 1971) that in sea urchin sperm flagella the active moments can be explained by this summing over the entire length of the fibers.

In the effective and in the recovery stroke of cilia the active moments are alternately of positive and negative direction. It has been generally assumed that the peripheral fibers on one side and on the other side are alternately activated to produce

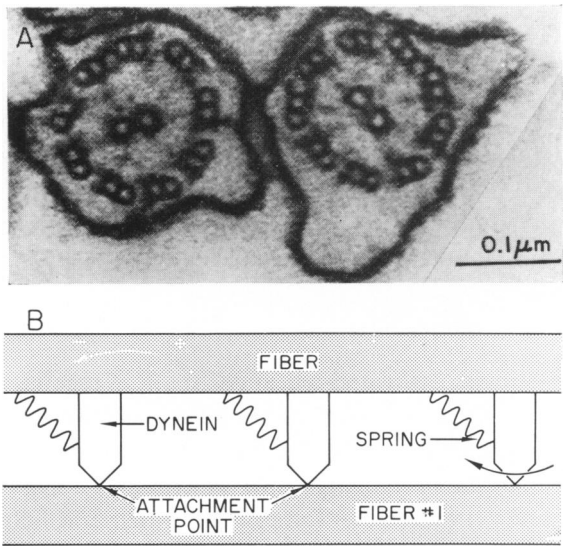

FIGURE 12 (A) Cross sections of two axonemes. The nine peripheral fibers, each consisting of a double tubule with projecting dynein arms are clearly visible. The central pair of fibers is also shown (courtesy of Dr. B. Afzelius). (B) Diagrammatic presentation of a sliding filament mechanism in cilia (reprinted from *Biophys. J.* **11**:456).

the required forces. We will proceed here taking this assumption to be correct. The *Sabellaria* cilium is made up of 25–30 components, each of which has the structure depicted in Fig. 12 A. We will take the number of components to be 30 in all of our calculations below.

Effective Stroke

Within 3 ms after the onset of the effective stroke the full active moment is developed over the entire length of the cilium. If all the dyneins on the fibers at the side which powers the effective stroke are activated, the moment is given by

$$M_{\text{eff}}(s) = m_e D_0 \int_s^L \sigma(s)\, ds, \qquad (13)$$

where m_e is the moment produced by one dynein molecule, D_0 is the density of dynein molecules per unit length of the cilium at the base ($s = 0$), and $\sigma(s)$ is the distribution of dyneins along the cilium, normalized to that at the base.

We do not know the nature of the signal that triggers the activation of the effective stroke. It has been shown (Rikmenspoel and Sleigh, 1970) that a mechanical impulse could not travel the length of the cilium within the 3 ms during which the active moment rises from zero to full intensity. Probably an electrical or chemical signal is involved (compare the review by Kinosita and Murakami, 1967). We shall not speculate on this, however, because the present work cannot reveal anything about these signals.

At the base ($s = 0$) of the *Sabellaria* cilium, with 30 components each having four fibers activated in the effective stroke, the density of the dynein molecules (with a pair on each fiber at 170 Å interval) is $D_0 = 1.41 \times 10^8$ dyneins/cm.

The *Sabellaria* cilium, when viewed under the microscope, is tapered towards the tip.[1] This means that some of the axonemes present at the base terminate before the end of the cilium. The density $\sigma(s)$ of dynein molecules is therefore not uniform along the cilium. From Eq. 13 we find with Eq. 12

$$(\mathrm{d}M/\mathrm{d}s) \propto \sigma(s) = (1 - s/L)^{0.75}.$$

The diameter of the cilium, as it appears under the microscope, is proportional to $\sigma(s)^{1/2}$ or diam $\propto (1 - s/L)^{0.375}$. Fig. 13 shows the shape of M_{act}, $\sigma(s)$, and the diameter of the cilium. Unfortunately no data exist in the literature on the change of diameter of this cilium along its length. We have noted, however, that the profile for the diameter of Fig. 13 resembles the profile for the morphologically somewhat similar cilium of *Mytilus*, published by Baba and Hiramoto (1970). To obtain an active moment at the base ($s = 0$) of 3.8×10^{-8} dyn cm, requires from Eq. 13, with the above values for D_0 and $\sigma(s)$, a moment per dynein molecule $m_e = 1.5 \times 10^{-13}$ dyn cm.

For the flagellum of sea urchin sperm one of us has found from small amplitude analysis of the wave motion a value of the active moment at the proximal end of 1.8×10^{-9} dyn cm (Rikmenspoel, 1971). The same mechanism as in the *Sabellaria* cilium, the activation of the fibers over their entire length was proposed for these flagella. Where these sperm flagella consist of a single axoneme (9 + 2 fibers), $\sigma(s) = 1$ and $D_0 = 4.7 \times 10^6$ dyneins/cm. This corresponds for sea urchin sperm to a value of $m_e = 1 \times 10^{-13}$ dyn cm. The closeness of the values for m_e for these different structures and obtained with different analyses gives confidence that the basic assumptions in both cases are correct.

According to Fig. 7 full activation is maintained in the *Sabellaria* cilium for a period t_{act} of approximately 15 ms, after which it decays. Fig. 7 shows that at 24 ms part of the active moment is still intact. In the data of Fig. 1 we also observe that in the real cilium a downward movement of the tip persists after 24 ms, which indicates that the active moment of the effective stroke does not abruptly vanish at 24 ms. This suggests an exponential decay of the active moment, with decay time τ_{eff}. The expression for the active moment thus becomes

$$\begin{aligned} M_{\mathrm{eff}}(s, t) &= f_{\mathrm{eff}}(t) m_e D_0 \int_s^L \sigma(\xi)\, \mathrm{d}\xi \\ f_{\mathrm{eff}}(t) &= 1 \qquad (t < t_{\mathrm{act}}) \\ f_{\mathrm{eff}}(t) &= \exp\{-(t - t_{\mathrm{act}})/\tau_{\mathrm{eff}}\} \qquad (t > t_{\mathrm{act}}). \end{aligned} \tag{14}$$

[1] Private communication by Dr. M. A. Sleigh.

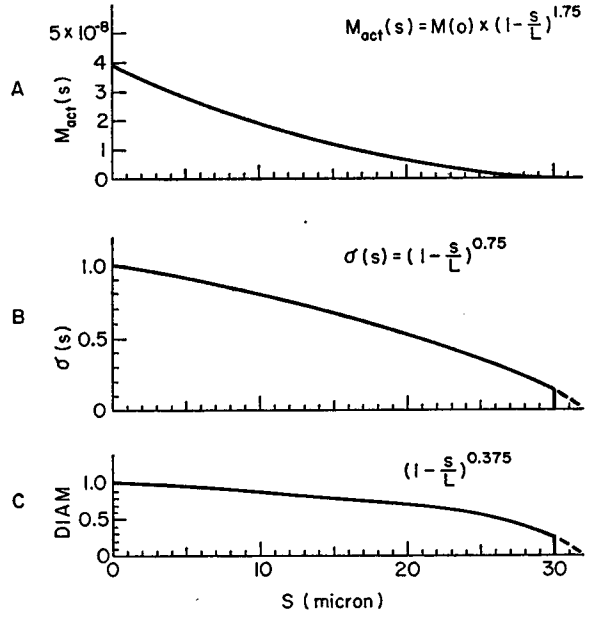

FIGURE 13 (A) Shape of active moment along the length of the cilium during the initial phase of the effective stroke (3–12 ms) of *Sabellaria*. (B) Distribution $\sigma(s)$ of dynein molecules on the *Sabellaria* cilium, as derived from the shape of the active moment. The most distal 2 μm of the cilium are assumed to be inert. (C) Diameter of the compound cilium corresponding to the distribution of dyneins shown. For further explanation see text.

τ_{eff} can be interpreted as the kinetic constant for the loosening of the dynein attachment. It may also represent the decay of the activating signal, however.

The iteration procedure of the preceding section has shown that the stiffness of the *Sabellaria* cilium decreases with the active moment. It is lowest in the distal part of the cilium during the recovery stroke. We take this lowest value, where the dyneins are apparently not attached, to represent the elasticity of the matrix material of the cilium and the membranes: $IE_{mat} = 1.8 \times 10^{-13}$ dyn cm^2.

When the dyneins are attached, the peripheral fibers are not free to slide, and the fibers then contribute to the stiffness. We can thus write

$$IE(s, t) = IE_{mat} + IE_{fibers} f(t) \sigma(s), \qquad (15)$$

where IE_{fibers} represents the stiffness at the base ($s = 0$) due to the peripheral fibers. The value for the total stiffness at the base ($s = 0$) of the cilium, during the beginning of the effective stroke, $IE = 3 \times 10^{-12}$ dyn cm^2, gives from Eq. 15 $IE_{fibers} = 2.8 \times 10^{-12}$ dyn cm^2.

The stiffness is a "local" property. The variation of the stiffness with time and position on the cilium as expressed by Eq. 15 is an essential property of a sliding

filament mechanism: where the fibers are free to slide, they do not contribute to the stiffness, where dyneins bind them together they do contribute.

It should be noted also that the stiffness of the fibers of one component of the *Sabellaria* cilium when fully activated ($\approx 10^{-13}$ dyn cm^2) is close to the value for the fibers of the sea urchin sperm flagellum, which has been reported as 0.6×10^{-13} dyn cm^2 (Rikmenspoel, 1966) and 0.9×10^{-13} dyn cm^2 (Rikmenspoel, 1971).

The fact that the *Sabellaria* cilium, with 30 axonemes, appears approximately 30 times stiffer than the sea urchin sperm flagellum, which is a single axoneme, shows that the component axonemes of *Sabellaria* are free to slide over each other during bending. This sliding of the components of a compound cilium should not be confused with the processes in a "sliding filament mechanism." These latter take place *inside* one component, between the peripheral fibers.

If the peripheral fibers are yielding to stretching under the influence of the forces present, their stiffness contribution is not a strictly local property, but it is averaged over a distance δs. In that case we can write

$$IE(s, t) = IE_{\text{mat}} + IE_{\text{fibers}} f(t) \int_s^{s+\delta s} \sigma(s)\, ds(1/\delta s). \qquad (16)$$

As was discussed above (see also Fig. 11) the iteration of the recovery stroke indicated that the change in stiffness along the cilium is not abrupt. Our computer program has in effect a "spacial resolution" of 2 μm. We have therefore adopted Eq. 16 as describing the stiffness in our calculations with a value of $\delta s \geq 2\mu$m. Unless mentioned otherwise we have used $\delta s = \Delta s$ ($= 2$ μm for *Sabellaria*).

Recovery Stroke

We want the same contractile mechanism as used in the effective stroke to apply to the recovery phase. Only the way activation of the contractile molecules is brought about is different during the latter. The results of the iteration in the preceding section clearly shows that contractile activation is induced by the traveling bend of the cilium. This activation can be caused by a bend in the fibers or by sliding of the fibers relative to each other. In Fig. 1, however, we observe that in the period 36–48 ms a clear bend is present in the proximal part of the cilium, whereas there is no motion there that is indicative of the development of a newly induced moment. We believe therefore that the activation is caused by the sliding of filaments. This agrees with the fact that sliding only occurs in the traveling bend in the more distal part of the cilium, and not in the bend near the base.[2] The idea of activation by sliding of the filaments has, in a different form, also been proposed in sea urchin sperm by Brokaw (1972 *a*, *b*); this will be referred to in the section Discussion. The model of A. F.

[2] It is an entertaining experiment to try out by means of, for example, a telephone directory where and when sliding occurs during the recovery stroke.

Huxley (1957) for skeletal muscle also contains an actin-myosin binding which is dependent on sliding.

We can exclude the possibility that tension in the fibers is the cause of an "autocatalytic" activation. In the proximal 8 μm of the cilium (Fig. 1) tension is present but there is no indication of the new development of active moment at 36–48 ms. Furthermore, when the fibers are not cross-linked, as in the distal part of the cilium, bending does not result in (elastic) tension in the fibers.

If activation is caused by sliding, it will persist as long as sliding occurs. This is in our present case as long as it takes the bend to pass over the location of the cilium under consideration. After the bend has passed sliding and activation cease and the dynein attachment will decay with a decay time τ_{rec}. We cannot a priori assume that $\tau_{rec} = \tau_{eff}$, because we do not know that τ_{eff} is determined only by the kinetics of the dynein-tubulin interaction. Later on we will indeed find that the shapes of the *Sabellaria* cilium cannot be reproduced with $\tau_{rec} = \tau_{eff}$.

If the time at which the bend of the recovery stroke *starts* to develop is called t_0, we find from Fig. 1: $t_0 = 12$ ms. The velocity of the progression of the bend along the cilium $v = 650\ \mu$m/s according to Fig. 1. At time t, activation of the contractile process in the recovery stroke therefore starts at a location $s_b = v(t - t_0)$ from the base. If the length of the bent section in which sliding occurs is called Δ, activation terminates at the point $v(t - t_0) - \Delta$ from the base. From Fig. 1 we have taken $\Delta \approx 6.5\ \mu$m.

At a point ξ on the cilium, at time t, we thus find for the activation $f_{rec}(\xi, t)$:

$$f_{rec}(\xi, t) = 0, \qquad v(t - t_0) < \xi < L,$$

$$f_{rec}(\xi, t) = 1, \qquad v(t - t_0) - \Delta < \xi < v(t - t_0),$$

$$f_{rec}(\xi, t) = \exp\left\{-\left(t - t_0 + \frac{\xi - \Delta}{v}\right) \Big/ \tau_{rec}\right\}, \qquad 0 < \xi < v(t - t_0) - \Delta. \quad (17)$$

During the recovery stroke the real drag coefficient is, as discussed above, probably higher than in the effective stroke. Furthermore, we cannot a priori assume that the activation by sliding in the recovery stroke has exactly the same intensity as the activation by a signal in the effective stroke. In calculating active moments with the activation given in Eq. 17 we have therefore multiplied the activation by a parameter α, to be adjusted as necessary. For the model to be meaningful, we do require, however, that α be near unity (even though probably less than 1), and that it is not dependent on s or t. The active moment for the recovery stroke becomes:

$$M_{rec}(s, t) = -\alpha m_e D_0 \int_s^L f_{rec}(\xi, t)\sigma(\xi)\, d\xi, \quad (18)$$

m_e, D_0, and $\sigma(\xi)$ are identical with those in the effective stroke.

When $M_{rec}(s, t)$ as defined in Eq. 18 is calculated, its shape and magnitude do

indeed resemble those shown in Fig. 11. Near the base the calculated shapes vary with the value for τ_{rec} adopted. The total active moment, from Eqs. 14 and 18 becomes

$$M_{act}(s, t) = M_{eff}(s, t) + M_{rec}(s, t).$$

The contribution of the peripheral fibers to the stiffness due to the recovery activation is

$$IE_{rec}(s, t) = \alpha IE_{fibers} \int_{s}^{s+\delta s} f_{rec}(\xi, t)\sigma(\xi)\, d\xi(1/\delta s) \qquad (19)$$

It should be noted that the stiffness is an inherently positive quantity, and that Eq. 19 has no negative sign. The total stiffness is the sum of the expressions given in Eqs. 16 and 19.

APPLICATION OF THE MODEL TO *SABELLARIA*

When we apply the model developed above to generate the motion of the *Sabellaria* cilium, the values of the decay times τ_{eff} and τ_{rec} have to be determined. This can only be done by investigating how the generated motion is dependent on these constants.

The motion of the cilium computed with the model (see Fig. 17 below) does not differ much from that obtained in the iteration procedure (Fig. 9) in the period 0–12 ms. Reduction of the stiffness towards the tip of the model results, according to Fig. 17, in a somewhat better representation of the curvature near the tip at 9 and 12 ms (cf. Fig. 1).

Near the end of the effective stroke (t = 24 ms), the downward motion of the distal part of the cilium depends on τ_{eff}. In the calculations reported below, we have adjusted the time during which full activation persists (t_{act}), such that for every τ_{eff} the position at 24 ms was close to the one of Fig. 1. Fig. 14 B shows how t_{act} varies with τ_{eff}.

Fig. 14 A shows the position of the tip of the computed cilium in the period 18–30 ms as a function of τ_{eff}. It can be seen that when $\tau_{eff} > 7$ ms too much overshoot of the tip relative to its position at 24 ms is present. From Fig. 14 we have adopted a value of τ_{eff} = 5 ms. For this value the match with the experimental positions is almost perfect. The value of τ_{rec} has no influence on the results shown in Fig. 14. At t = 30 ms the decay of contractility of the recovery stroke has nowhere started yet.

Fig. 17 below shows the complete effective stroke computed with the model at τ_{eff} = 5 ms. The representation of details such as the curvature in the distal part in the latter period of the stroke ($t > 12$ ms) and the relative spacing of the consecutive positions is better than that obtained from the iteration procedure (Fig. 9), and it is certainly as good as can be expected from a very simple model.

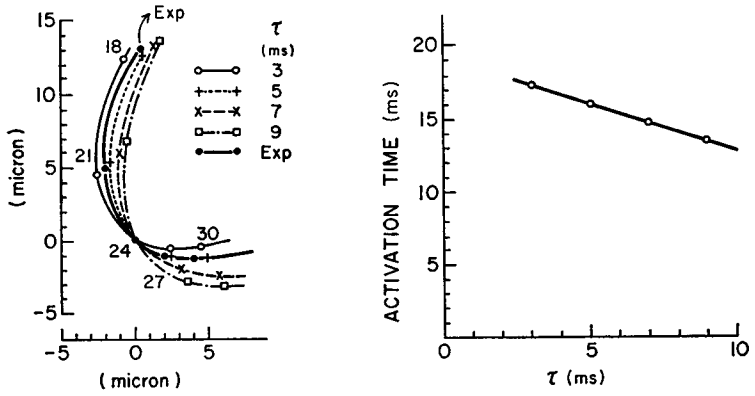

FIGURE 14 (A) Path followed by the tip of the model cilium in the period 18–30 ms, computed for various values of the decay time τ_{eff} of the contractile activity. (B) Value of the activation time τ_{act} adopted as function of the decay time τ_{eff}.

Recovery strokes (24–60 ms) which have a bend traveling at the correct speed are obtained with all values for τ_{rec} between 5 and 30 ms. The shape of cilium proves to be very sensitive to the value of τ_{rec} used.

In all calculations the value of the parameter α in Eq. 18 was adjusted so that the envelope of the positions of the cilium in the latter period of the recovery stroke was parallel to the y axis (compare Fig. 1). In practice the value of α varied from 0.5 at $\tau_{rec} = 5$ ms to $\alpha = 0.4$ at $\tau_{rec} = 30$ ms. When α is taken too big the envelope of the recovery stroke will tip "downwards," when α is too small the envelope will point upwards. In the section Iteration in Time for *Sabellaria*, we have seen that the difference in drag coefficient between the effective and the recovery strokes could be as much as a factor of two. The fact that $\alpha \approx 0.5$, without much variation for the different τ_{rec}'s, suggests therefore that α in Eqs. 18 and 19 mainly corrects for the change in drag coefficient and that the activation by sliding is approximately as intense as the activation by signal during the effective stroke.

Fig. 15 shows two recovery strokes, computed with $\tau_{rec} = 5$ ms and $\tau_{rec} = 25$ ms, respectively. The distance of the horizontal part of the envelope of the stroke to the cell surface (the y axis) is much too large at $\tau_{rec} = 5$ ms. This can be understood as being due to too fast a decay of the contractility near the base, with the result that not enough moment is left to bend the cilium over.

The distance of the envelope of the recovery stroke from the cell surface (the "roll off" height) decreases when τ_{rec} is larger as shown in Fig. 16. For $\tau_{rec} \geq 15$ ms the roll off height is 3–4 μm, compatible with the data of Fig. 1.

The curvature in the bend on the cilium increases with the value of τ_{rec}. The curvature is not constant along the bent section, but the maximum curvature which occurs at the distal end of the bend, is for all values of τ_{rec} approximately equivalent to a $\rho = 4$ μm.

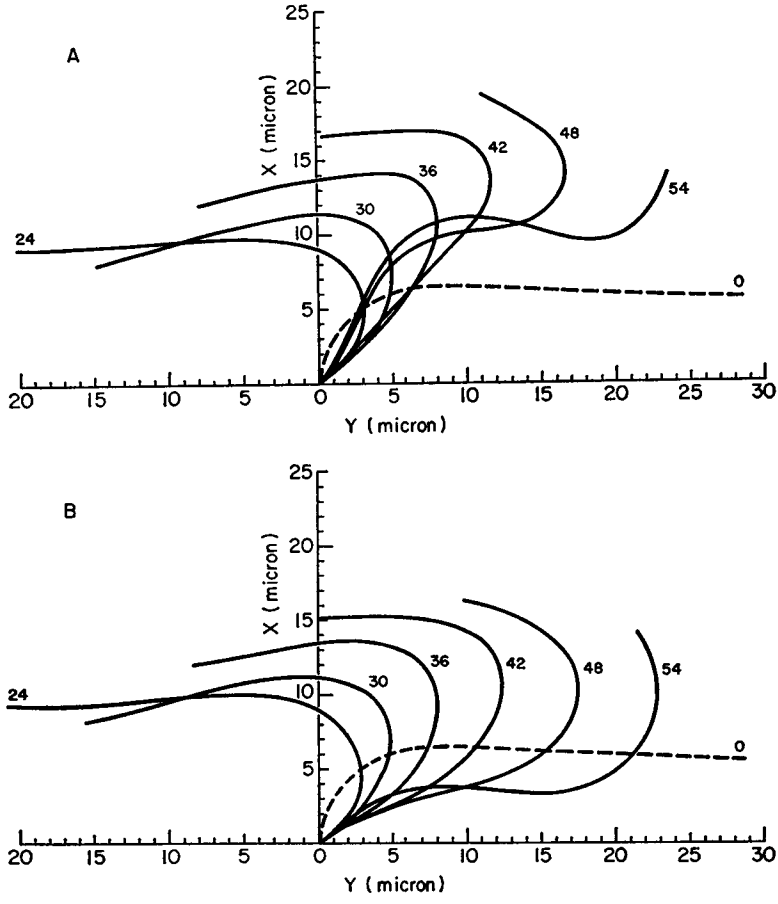

FIGURE 15 (A) and (B) Recovery stroke computed for the model cilium with different decay times of contractile activity. (A) $\tau_{rec} = 5$ ms; (B) $\tau_{rec} = 25$ ms.

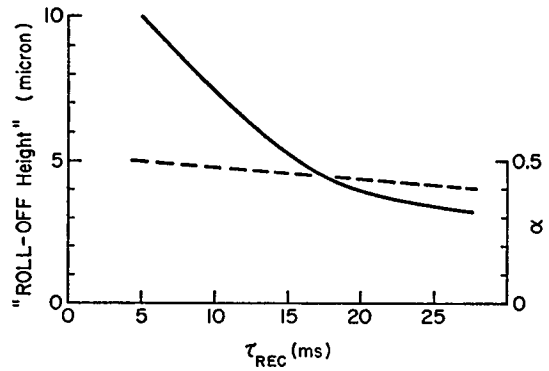

FIGURE 16 Height above the cell surface at which the computed recovery stroke rolls off, as a function of τ_{rec}. The dotted line shows the value of α adopted as a function of τ_{rec}.

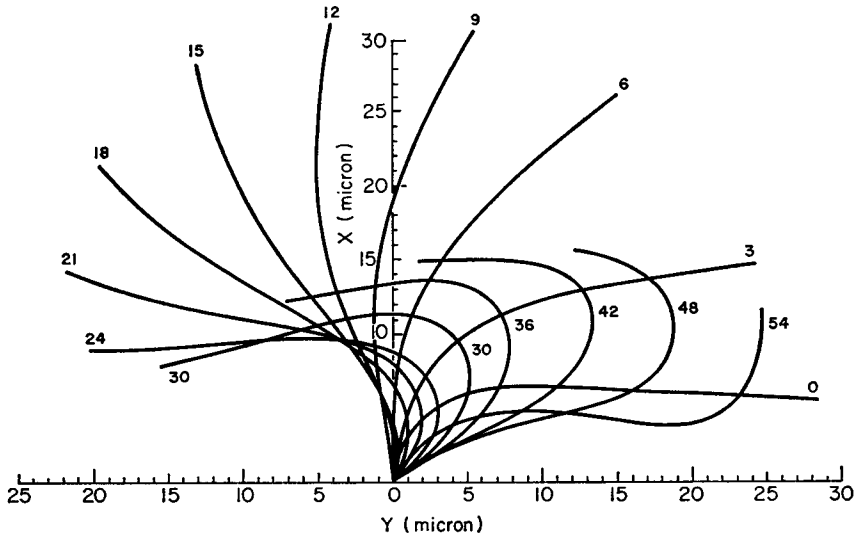

FIGURE 17 Full cycle of the model *Sabellaria* cilium computed with $\tau_{eff} = 5$ ms and $\tau_{rec} = 20$ ms.

The best shape of the recovery stroke is obtained with $\tau_{rec} = 20$ ms. The complete ciliary stroke computed with $\tau_{eff} = 5$ ms and $\tau_{rec} = 20$ ms is shown in Fig. 17. It is somewhat difficult to define objective criteria by which a "best" shape can be judged. However, the overall appearance of the computed recovery stroke of Fig. 17 gives a smoother impression than those obtained with different values for τ_{rec}, and illustrated in Fig. 15.

Figs. 18 and 19 give contour plots for the total active moment and for the stiffness of the cilium during the complete cycle. The general characteristics of the moments and stiffness, as a function of s and t, found in the section Iteration in Time for *Sabellaria* are present in these contour plots. The strongly varying shape during the cycle of the moment and of the stiffness indicates that analytic solutions for the equation of motion for the case of cilia can be considered excluded.

The main deviation of the model cilium in Fig. 17 from the data of Fig. 1 is the fact that during the recovery stroke the tip of the cilium moves at approximately 15 μm from the cell surface, instead of at approximately 11 μm from it as in Fig. 1. We have tried to get a better fit for the path of the tip of the cilium by varying the value for the quantities involved in calculating the stiffness. The calculations were started at $t = 24$ ms.

Variation of the value of IE_{mat} or IE_{fibers} of Eq. 16 by up to a factor of two smaller results in a more "pointed" bend, increasing these values results in a recovery stroke like the one shown in Fig. 15 B. Increasing δs of Eq. 19 to up to 4 μm has almost no effect, when $\delta s > 6$ μm a more pointed bend is obtained. In all these cases the smooth appearance of the computed recovery stroke is largely lost, and the motion of the tip of the cilium remains at a distance of 14–15 μm from the surface.

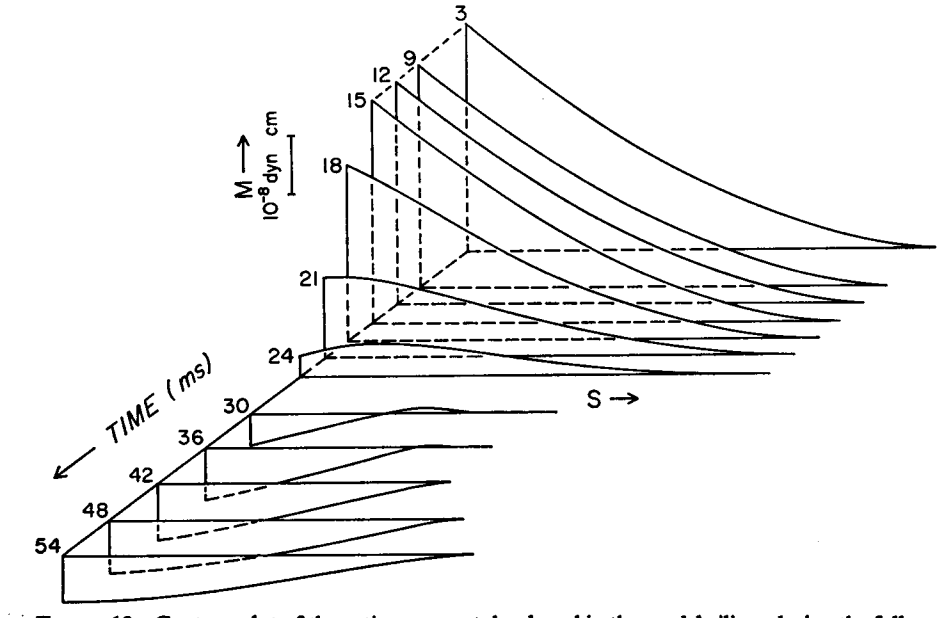

FIGURE 18 Contour plot of the active moment developed in the model cilium during the full cycle.

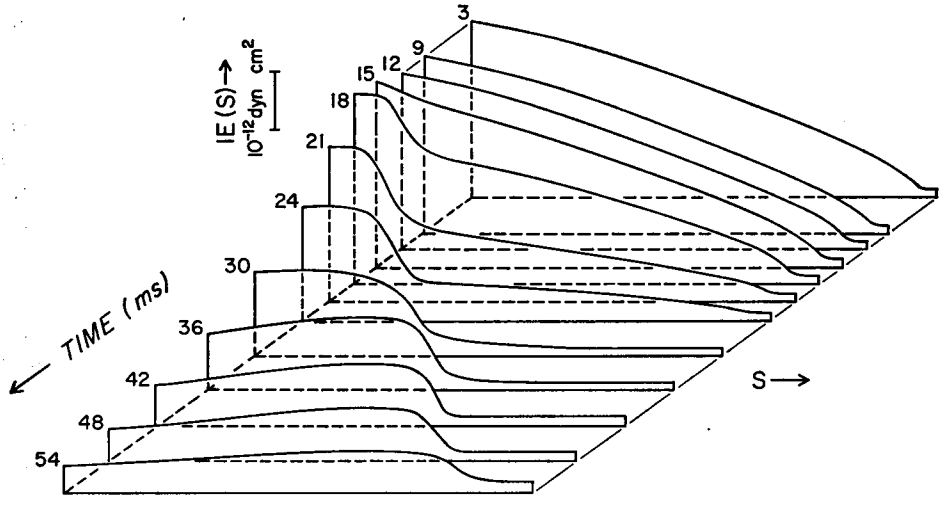

FIGURE 19 Contour plot showing the stiffness of the model cilium as a function of location on the cilium during the full cycle.

Variation of the form of $\sigma(s)$ does not have much influence on the shape of the recovery stroke up to $t \approx 45$ ms. This is understandable because it is the density of dyneins near the tip of the cilium which is mainly varied by changes in $\sigma(s)$, and during most of the recovery stroke the distal part of the cilium is not activated. In

the section Iteration in Time for *Sabellaria* it was already observed that the effective stroke cannot be well represented with a different form of $\sigma(s)$.

The deviations of the shape of the recovery stroke of the model are therefore not due to errors in our estimates of stiffness and distribution of dynein molecules. Since all of the above trials were unsuccessful a detailed presentation does not seem warranted.

We have concluded from the above that the deviations from the data for the recovery stroke are caused by a too great simplicity in the way the activation of the contractile elements in the recovery stroke is prescribed in our model. The point at which activation starts, see Eq. 17, is assumed to progress with a constant velocity $v = 650\ \mu m/s$. A measurement from Fig. 1 shows (Rikmenspoel and Sleigh, 1970) that v varies as the bend travels along the flagellum. The length of the bend during which sliding, and therefore activation, occurs is taken to be constant in the model. Fig. 1 indicates that this also is a simplification.

The correct formulation can only be obtained if after every iteration step the locations where sliding begins and stops are calculated. This involves an evaluation of the zero points of the expression

$$\int_0^s \frac{\partial}{\partial t}\left[\frac{\partial\theta(\xi)}{\partial\xi}\right] d\xi \qquad (20)$$

over the cilium. Accurate computation of the expression of Eq. 20 would require at least a four times smaller length interval Δs than the one used ($\Delta s = 2\ \mu m$). Since the computing time required for one iteration step increases with approximately the third power of the number of length intervals, these calculations are not within the capacity of our available computer. Even if such a refinement were feasible, it is doubtful whether new insight would be obtained, as long as better expressions for the drag coefficient at every stage of the ciliary cycle are not available.

OTHER TYPES OF CILIARY MOTION

The model developed above lends itself to application to the motion of cilia of other species. To this end we shall consider again the equation of motion (Eq. 6), and the model defined by Eqs. 14, 16–18. Since we have found that the components of the compound *Sabellaria* cilium are free to slide over each other, the stiffness IE of a compound can be written as $IE = Nie$ where N is the number of component axonemes (9 + 2 structures) and ie is the stiffness of one axoneme.

For our model we find

$$ie(s) = ie_{\text{matrix}} + ie_{\text{fibers}} \int_s^{s+\delta s} \alpha f(\xi, t)\sigma(\xi)\, d\xi (1/\delta s)$$

where $ie_{\text{matrix}} = 6 \times 10^{-15}$ dyn cm^2 and $ie_{\text{fibers}} = 9.4 \times 10^{-14}$ dyn cm^2 are the stiffness values for the matrix and peripheral fibers of one component. $f(\xi, t)$ is $f_{\text{eff}}(t)$ from

Eq. 14 for the effective stroke or $f_{rec}(\xi, t)$ from Eq. 17 for the recovery stroke; $\alpha = 1$ for the effective stroke and $\alpha = 0.5$ for the recovery stroke.

If we rewrite the equation of motion in a dimensionless coordinate $z = s/L$ (with z varying from 0 to 1), the elastic term in Eq. 6 becomes

$$(N/L)ie(z)(\partial\theta/\partial z). \tag{21}$$

The active moment becomes

$$M_{act}(z, t) = NLm_c D \int_z^1 \alpha f(\xi, t)\sigma(\xi)\, d\xi \tag{22}$$

where $D = 4.7 \times 10^6$ dyneins/cm is the density of dyneins for one component axoneme.

The viscous moment written out in Eqs. 3 and 4 is proportional to L^3, and using the notation of Eq. 5,

$$M_{visc}(z, t) = kL^3 M(\partial\theta/\partial t, \cos\theta, \sin\theta). \tag{23}$$

The drag coefficient k in Eq. 23 varies with the number of components. According to Eqs. 10 and 11 we can expect this variation to be weak.

The terms of Eqs. 21–23 define the new equation of motion. In the sections in which the model was developed we have learned that during the effective stroke the stiffness term of Eq. 21 is smaller in magnitude than the active moment and the viscous terms of Eq. 22 and 23. The latter two are therefore dominant in the equation of motion and should be very roughly equal in the effective stroke.

The length of cilia and the number of component axonemes varies greatly for various species, but the duration of the effective stroke is usually from 15 to 50 ms (Sleigh, 1968). We would from the rough equality of M_{act} and M_{visc} in the effective stroke, together with Eqs. 22 and 23, therefore expect kL^2/N to be a constant for various cilia.

Table II lists the parameters for several ciliary structures, varying a factor of 60

TABLE II

LENGTH L, NUMBER OF COMPONENT CILIA N, DRAG COEFFICIENT k AND SCALING FACTOR kL^3/N FOR CILIA OF FIVE DIFFERENT SPECIES

Organism	L	N	k	kL^3/N
	cm	*no. of components*	*dyn cm^{-2} s*	*10^{-8} dyn s*
Paramecium	0.0010	1	0.028	2.8
Stentor	0.0028	60 (40–75)	0.057	0.75
Sabellaria	0.0032	30	0.037	1.3
Jorunna	0.0046	?	0.037	—
Pleurobrachia	0.0600	several $\times 10^5$ $(2–3) \times 10^5$	2.0	(3.6–2.4)

length and a factor 10^5 in number of components. Within the very large range the factor kL^2/N is practically constant. This type of "scaling" behavior has been pointed out before in a somewhat different way by Harris (1961).

The "scaling factor" N/L for the elastic term, Eq. 21, is quite different from that for the active and viscous terms in Eqs. 22 and 23. Since the shape of the cilium is sensitive to the stiffness, the model formulated in Eqs. 21–23 can be meaningfully tested by applying it to cilia with different length L and number of components N.

Of the cilia in Table II the shape during the cycle has been presented in a more or less diagrammatic way by Sleigh (1962, 1968) for *Paramecium*, *Jorunna*, and *Stentor* (Figs. 20–22). The effective stroke was in all three cases indicated by straight lines. No information is therefore contained in these representations of the effective stroke.

The recovery stroke for the three cilia in Figs. 20–22 is given in more detail. The shape and the duration of the recovery are very different in the three cases, and they should therefore provide a test for our model.

For the macroscopic structure of the comb plate of *Pleurobrachia* a detailed and accurate description of the motion during the cycle has recently been obtained by Sleigh and Jarman (1973),[3] shown in Fig. 23 below. Unfortunately our knowledge of the drag coefficient and its variation during the cycle and along the cilium is poor for this particular case, and a precise testing of the model over the entire cycle is impossible. This is explained in more detail below as the various cases are treated.

For application of the model to the four cases mentioned above, the length of the structure is known accurately in each case. The velocity at which the recovery bend travels, and the length of the bend can be measured with a ruler from the diagrams in Figs. 20–23. α was maintained equal to 1 for the effective stroke and equal to 0.5 for the recovery stroke. The function $\sigma(z)$ was used in the same form as that for *Sabellaria*: $\sigma(z) = (1 - z)^{0.75}$ since no knowledge of a more precise nature exists. For the case of *Paramecium*, however, it is known that the cilium is not a compound but a single (cylindrical) 9 + 2 structure. In this case only we have as a consequence taken $\sigma(z) = 1$.

In the application of the model to *Sabellaria* it has been found that the shape of the recovery stroke is not very sensitive to the exact form of $\sigma(z)$. Our lack of information on $\sigma(z)$ is therefore not very serious.

The values obtained from *Sabellaria*, $m_e = 1.5 \times 10^{-13}$ dyn cm, $\tau_{ett} = 5$ ms, $\tau_{rec} = 20$ ms, have been maintained throughout. Our model is therefore left with one parameter: N, the number of component axonemes. In testing the model we have computed return strokes with various values of N, starting near the beginning of the recovery stroke. For the cases of *Jorunna* and *Stentor* the recovery stroke

[3] We wish to thank Dr. Sleigh for his gracious permission to use the data on *Pleurobrachia* before publication.

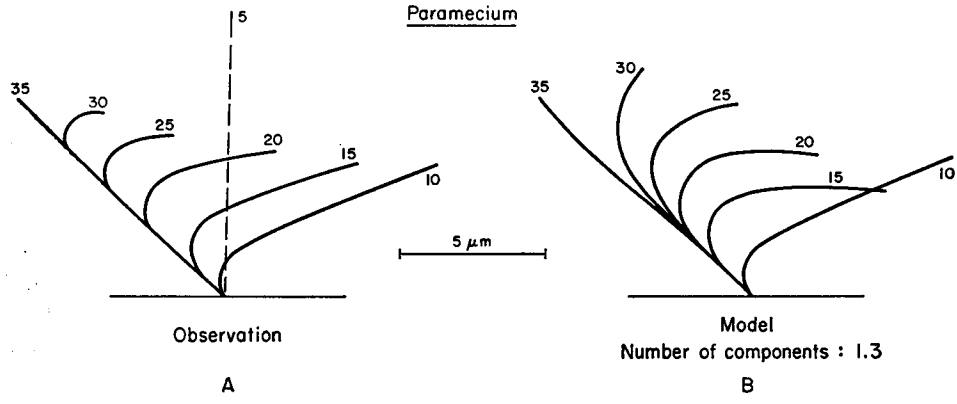

FIGURE 20 (A) Motion of the cilium of *Paramecium* during complete cycle at 5 ms intervals (courtesy of Dr. M. A. Sleigh). (B) Recovery stroke computed for a model with 1.3 axonemes.

overlaps with the effective stroke. The end of the effective stroke was therefore included in the calculations. Each of the cases is discussed in more detail below.

Paramecium

The cilium of *Paramecium* is a short ($L = 10$ μm) single axoneme. The motion at intervals of 5 ms is shown in Fig. 20 A (from Sleigh, 1968). No "overlap" seems to be apparent between the effective and the recovery stroke according to Sleigh (1968). We have therefore started the calculations with the position at 10 ms, taking $f_{eff}(t) = 0$.

The cilium is cylindrical [$\sigma(z) = 1$], with a diameter 0.2 μm. From Fig. 20 A the length of the bend section $\Delta \approx 3$ μm. According to Eq. 10 the drag coefficient, using the values $a = 0.1$ μm and $\lambda = 2\Delta = 6$ μm, is $k = 0.028$ dyn cm^{-2} s. The velocity at which the bend propagates is from Fig. 20 A, $v = 300$ μm/s.

The recovery stroke was computed for various values of N (the number of axonemes). The best fit, obtained with $N = 1.3$, is shown in Fig. 20 B. The value $N = 1.3$ is close to the experimental value of 1. Even though the distal part of the cilium lags a little in the model compared with the data, the general shape of the recovery stroke is well reproduced.

Stentor

The *Stentor* cilium is a "membranelle," built up of "two to three rows of 20–25 cilia each" (Sleigh, 1962). The cross section has dimensions of approximately 5×0.7 μm (Sleigh, 1962).

Two diagrams of the motion of the *Stentor* membranelle are shown in Fig. 21 A (Sleigh, 1968) and Fig. 21 B (Sleigh, 1962). As an average from these two diagrams we have adopted values of $\Delta = 9$ μm and $v = 1170$ μm/s.

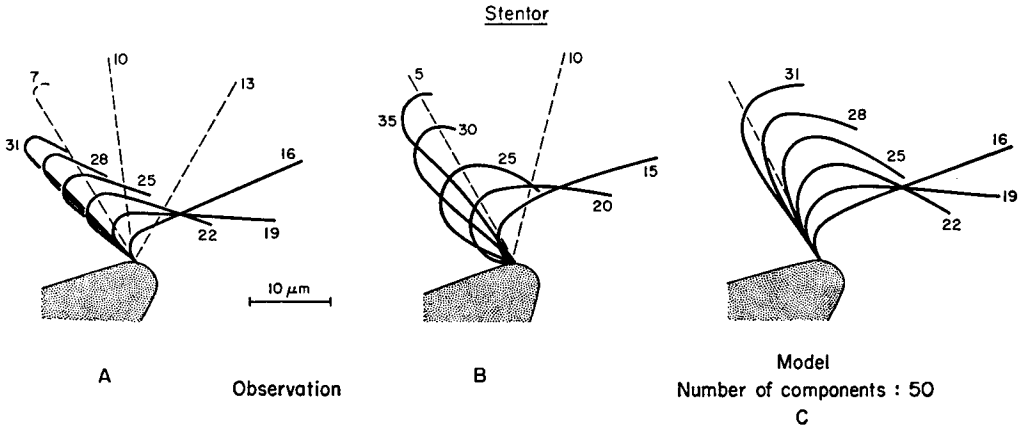

FIGURE 21 (A and B) Two different observations of the motion of the *Stentor* cilium during a full cycle (courtesy of Dr. M. A. Sleigh). (C) Computed recovery stroke for a model with 50 axonemes.

For calculations of the viscous drag of a ribbon-like structure the appropriate dimension to be used is the width of the ribbon (Lamb, 1952). Taking for insertion into Eq. 10 $a = 2.5$ μm and $\lambda = 2\Delta = 18$ μm, we obtain for the drag coefficient $k = 0.057$ dyn cm^{-2} s.

The recovery phase of *Stentor* starts before a clear termination of the effective stroke (Fig. 21 A and B, and Sleigh, 1968). We have therefore started the model calculation at $t = 16$ ms, taking the end of the activation of the effective stroke $t_{act} = 11$ ms. This assures a resonable representation of the position at 22 ms.

The best shape of the recovery stroke, obtained with $N = 50$, is shown in Fig. 21 C. The value for N is well in the range (40–75) shown in Table II.

The shape in Fig. 21 C is a fair representation in view of the variation in observations shown in Figs. 21 A and B.

Jorunna

The compound cilium of *Jorunna* is rather long ($L = 46$ μm) and "flexible" (Sleigh, 1968). The motion is slow: the effective stroke has a duration of approximately 70 ms, the recovery stroke lasts approximately 100 ms. The number of component axonemes has not been reported in the literature.

Fig. 22 A shows the motion of the *Jorunna* cilium. The recovery stroke starts before the end of the effective stroke, as was the case with *Stentor* and *Sabellaria*. We have started the model calculations at $t = 55$ ms, using a value for $t_{act} = 60$ ms. This results in a fair representation of the position at 70 ms.

Since the number of components of the cilium is not known, the drag coefficient cannot be calculated. We have adopted the value of *Sabellaria* $k = 0.037$ dyn cm^{-2} s. From Fig. 22 A we have taken $v = 400$ μm/s, $\Delta = 9$ μm.

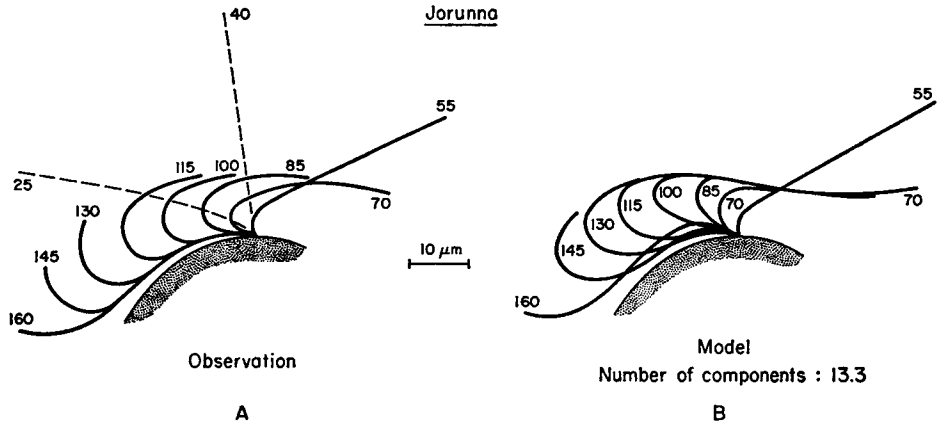

FIGURE 22 (A) Motion of the cilium of *Jorunna* during the complete cycle. Note the duration of the cycle of 160 ms (courtesy of Dr. M. A. Sleigh). (B) Computed recovery stroke for a model with 13.3 axonemes.

The best fitted recovery stroke, shown in Fig. 22 B, was obtained with $N = 13.3$. It can be seen that the fit is quite good.

The fact that a rather low value for N, in comparison to the length L, is found from the model, agrees well with the statement of Sleigh (1968) that the cilium is flexible and with the fact that the motion is slow.

Pleurobrachia

The comb plate of *Pleurobrachia* is a special case because it is a macroscopic sheet-like structure. A comb plate is built of up to 100 rows, each approximately 800 μm wide, of axonemes. The length $L \approx 600$ μm (Sleigh and Jarman, 1973). In total "several hundred thousand" axonemes are present.

Fig. 23 A shows the motion of the comb plate during one cycle (from Sleigh and Jarman, 1973). It can be seen from Fig. 23 A that in spite of the much larger dimensions the motion has the same general characteristics as the *Sabellaria* cilium.

A drag coefficient cannot be calculated with Eqs. 10 or 11 for a comb plate because its width is not small compared with the length. Instead these structures have more resemblance to a disk moving broadside on. The total viscous drag K for a cylindrical disk, moving broadside on is (Lamb, 1952)

$$K = 5.1\ \pi c\eta, \tag{24}$$

where c is the radius of the disk. Taking for c one-half of the average of the width and length of a comb plate ($c = 350$ μm), gives with Eq. 24 a value $K = 5.6 \times 10^{-3}$ dyne cm^{-1} s. If we assume that the drag is uniformly distributed over the disk, the viscous drag coefficient per unit length $k_{visc} = K/L = 9 \times 10^{-2}$ dyn cm^{-2} s.

A further complication is caused by the fact that the Reynolds number $R = VL/\nu$

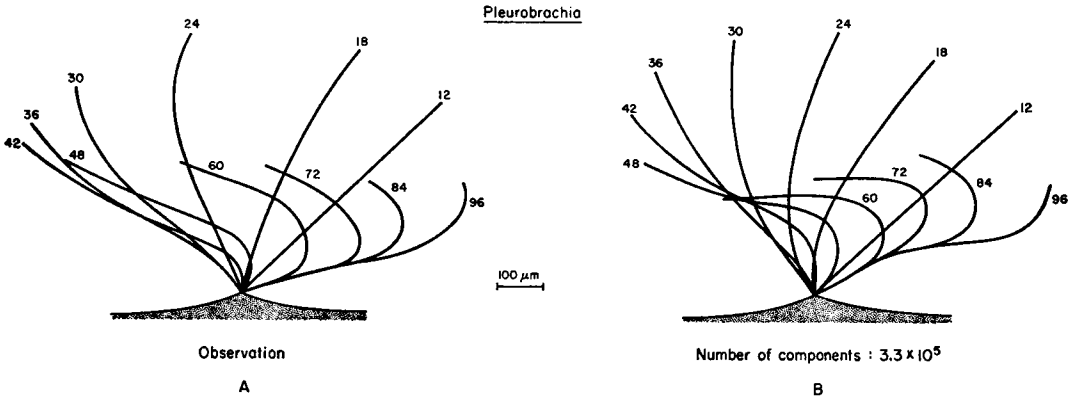

FIGURE 23 (A) Motion of the comb plate of *Pleurobrachia*. The comb plate is seen edge-on (courtesy of Dr. M. A. Sleigh). (B) Complete cycle computed for a model with 3.3×10^5 axonemes. For further explanation see text.

for the motion of a comb plate is not small. If we take for a characteristic velocity V the value in the effective stroke halfway along the structure ($V = 3$ cm/s), with $L = 0.06$ cm and $\nu = 1$ cSt, the Reynolds number becomes $R \approx 18$.

If we interpret the Reynolds number as the ratio of inertia to viscous forces (Sommerfeld, 1947), the total drag coefficient per unit length of the comb plate becomes $k = (R + 1)k_{\text{visc}}$, or (rounded off) $k \approx 2$ dyn cm^{-2} s.

The value for k derived above is, of course, a very rough approximation. A hydrodynamic theory which would allow a better estimate of k has not been developed, however. Where the "scaling law" illustrated in Table II appears to hold for the comb plate using $k = 2$ dyn cm^{-2} s, we have felt that this value is of the correct order of magnitude.

From Fig. 23 A we have taken the velocity of propagation of the bend during the return stroke $v = 7800$ μm/s, and the length of the bend $\Delta = 45$ μm. Computation for the model, with the above values for k, v, and Δ were started at the position at 12 ms, which is practically straight. We found that for any number of components N the model cilium buckles and collapses within a few milliseconds. If, however, the value of ie, the stiffness of a single axoneme of 10^{-13} dyn cm^2, is raised by a factor greater than 100, meaningful solutions are obtained for $N > 3 \times 10^4$. As in the case of *Sabellaria*, the curvature which develops during the effective stroke is mainly determined by the stiffness.

The best overall result is obtained with $ie = 5 \times 10^{-11}$ dyn cm^2, which is 500 times the value used for all other cases treated, and $N = 3.3 \times 10^5$. Fig. 23 B shows the complete cycle computed with these values. The activation during the effective stroke was terminated in Fig. 23 B at $t_{\text{act}} = 30$ ms.

Besides the facts that during the effective stroke the maximum curvature occurs in the proximal part in the model and in the distal part in the data, and also that in the

beginning of the recovery stroke the comb plate is too much bent over, the general shape of the cycle is reasonably represented. This shows that the mechanism for generating the active moment remains valid in this very large and rather slow organelle.

Electron microscopy (Afzelius, 1961) has revealed that two extra fibers (lamellae) are present in each axoneme of the comb plate. The fibers are located opposite each other outside the ring of the nine peripheral fibers in the plane perpendicular to the direction of motion. There is only a slight indication in the photographs presented by Afzelius that some of the cilia in a row are connected by a "dark substance." If the component cilia of the comb plate were free to slide over each other during the motion, all these extra structures are in the "neutral" plane and cannot contribute to the apparently greater stiffness.

Since no other elements have been found that could cause the extra stiffness, the probable explanation for it is that the component cilia are not totally free to slide over each other. The moments at the base of a comb plate are typically in the order of 10^{-1} dyn cm, compared with 10^{-8} dyn cm in *Sabellaria*. It seems reasonable to assume that the very much larger forces on the comb plate press the components together resulting in a friction which resists the sliding.

The stiffness of a solid plate is proportional to d^3, where d is the thickness. If the components of the comb plate, which has a typical $d = 20$ μm, were solidly bound together, the stiffness compared with the *Sabellaria* cilium (typically $d = 1$ μm) would be $\approx 10^4$ times higher. The stiffness increase of about 500 times can therefore be accounted for by a rather small amount of friction between the component cilia in the comb plate.

It should be kept in mind, however, that we cannot make any interpretation as to which structure (the peripheral fibers, or the two extra ones) is responsible for the stiffness of the comb plate. Table III shows the experimental values for the number of component cilia in the five structures treated in this paper, and the number of components used in the model.

TABLE III

NUMBER OF COMPONENT CILIA FOUND FROM OBSERVATION, AND FROM THE MODEL FOR FIVE DIFFERENT SPECIES

Organism of cilium	Number of components	
	Observation	Model
Paramecium	1	1.3
Stentor	40–75	50
Sabellaria	25–30	30
Jorunna	?	13.3
Pleurobrachia	several $\times 10^5$	3.3×10^5

DISCUSSION

It might be useful at this point to summarize the main features of the contractile model for cilia developed above.

(*a*) A sliding filament mechanism operates between the peripheral fibers. The dynein molecules form cross bridges between the peripheral fibers, each dynein producing an active moment of 1.5×10^{-13} dyn cm. The total active moment felt at location s is the sum of the moments produced by all attached dyneins distal to s.

(*b*) The peripheral fibers contribute to the stiffness of the cilium only when and where they are inhibited from sliding due to cross-linking by attached dyneins.

(*c*) The effective stroke is initiated by a signal which activates peripheral fibers over their entire length at once. After the signal ceases the contractile activity decays with a characteristic time $\tau_{eff} = 5$ ms.

(*d*) When peripheral fibers slide over each other the dyneins attach. After sliding ceases the attachment decays with a decay time $\tau_{rec} = 20$ ms. The moments produced this way are of such polarity that they tend to *decrease* the curvature that caused the sliding.

(*e*) In compound cilia the stiffness is the linear sum of the stiffness of the components. Only in very large structures (such as the comb plates) does a moderate amount of friction between components appear to exist.

The model contains five essential quantities: $m_e = 1.5 \times 10^{-13}$ dyn cm, the moment produced by one attached dynein, $D = 4.7 \times 10^6$ dyneins/cm, the number of dynein molecules on one "side" of an axoneme, *ie* $\approx 10^{-13}$ dyn cm^2, the stiffness of one axoneme where all dyneins are attached, and the two decay times τ_{eff} and τ_{rec}. Of these five quantities D is known beyond doubt from electron microscopy; it is the same in flagellar and ciliary axonemes. The estimates of m_e and *ie* obtained in this paper for ciliary axonemes are close to the values we have found earlier from a different analysis for sperm flagellar axonemes (Rikmenspoel, 1966, 1971).

An independent measurement of the two decay times τ_{eff} and τ_{rec} does not exist. At first sight it is indeed surprising that different decay times should apply to the two different ways of activating the dynein molecules. The effective stroke of *Paramecium*, however, appears to have completely terminated 10 ms after its start (Fig. 20 A and Sleigh, 1968). This cannot be reconciled with a decay time of the contractility much longer than 5 ms. On the other hand, the recovery stroke of *Sabellaria*, and even more, those of *Jorunna* and *Pleurobrachia*, cannot be represented with a decay time τ_{rec} smaller than $\approx$20 ms.

The model stands and falls therefore with the two different decay times. It is encouraging that recently Gibbons and Fronk (1972) have found evidence in dynein for two types of ATPase sites, one having a low and the other having a high ATP affinity. The two sites were observed in isolated axonemes in KCl concentration near those in intact organelles, with Mg^{++} activation. This observation lends

support to the idea that two types of kinetics can be present for the dynein-tubulin interaction.

In general, however, the fact that the model can explain the shape of ciliary strokes of a variety of durations and in a large range of sizes, is perhaps the best indication that the basic features of it are correct. We have in the section Other Types of Ciliary Motion not included rare or exotic types such as the cilia of *Mytilus*, of *Opalina*, and the cilium on the cephalic tentacle of *Sabellaria* (Sleigh, 1968). These species have in common that a clear separation between an effective and a recovery stroke is not present. The control of the ciliary activity is therefore different from that of the more normal types treated. A special investigation seems warranted for these rarer types mentioned above.

The calculations with our model strongly support the basic, nonlocal, nature of a sliding filament mechanism. The forces produced by dynein molecules are transmitted all the way to the point of attachment of the fibers. This indicates the special importance of the attachment of the fibers in the basal body of cilia or the centriole of flagella. Experimentally it has been found by Goldstein (1969) that after laser microbeam irradiation of the centriole area sea urchin sperm are not able to initiate new bending waves. Summers and Gibbons (1971) have found that broken, Triton-extracted sea urchin sperm flagella show wave motion upon ATP addition only in the fragments containing the centriole. Rikmenspoel and van Herpen (1969) have reported that the centriole of bull sperm is the area most sensitive for ionizing radiation. These observations would support the special role of the basal body or centriole as a mechanical anchor point for the contractile fibers.

In the above considerations of the model, we have been concerned only with the decay time of the contractile activity. At the beginning of the effective stroke (0–3 ms) of *Sabellaria* we have a clear indication that the attachment of the dynein molecules is not instantaneous. The characteristic time for dynein attachment is from Figs. 2 and 7 of the order of 1 ms. Together with a $\tau_{eff} = 5$ ms this means that during the period of full activity in the effective stroke ($\approx$16 ms) the dynein-tubulin binding has turned over several times.

During the recovery stroke the dynein-tubulin attachment probably also takes a finite time. Our relatively poor fit of the exact shape of the recovery stroke (Fig. 17) indicates, however, that no possibility exists to obtain estimates of the attachment time in that phase. We can therefore not say anything about possible turnover of the dynein-tubulin binding during the recovery phase.

The value for the stiffness of the distal part of the compound *Sabellaria* cilium during the recovery stroke (1.8×10^{-13} dyn cm^2) found in this paper is in agreement with the value of $(2 \pm 1) \times 10^{-13}$ dyn cm^2 obtained earlier (Rikmenspoel and Sleigh, 1970) from small amplitude elastic theory applied to the recovery stroke. This serves as an illustration of the power of small amplitude analysis when properly applied.

Finally, it might be of interest to compare the present findings on cilia with the proposals made for the coordination of contractility in flagella. From an analysis of the viscous and the bending moments in invertebrate sperm Rikmenspoel (1971) found that the active moment in these flagella was developed in phase over their length. The magnitude of the moment was found to decrease linearly along the length of the flagella. These observations led to the proposal that a sliding filament mechanism with summing of the moments produced by the dynein molecules operates in these flagella, with the fibers activated at once over their entire length.

In the effective stroke of cilia this mechanism of activation of the fibers over their entire length is directly displayed. The moment produced by one dynein molecule found by the analysis of the *Sabellaria* cilium ($m_e = 1.5 \times 10^{-13}$ dyn cm) is close to that found from the analysis of the sperm flagellar waves ($m_e \approx 1 \times 10^{-13}$ dyn cm).

In cilia the dynein-tubulin binding is activated also by sliding of the peripheral filaments. It is entirely possible that this process would also take place in a waving sperm flagellum. The moments produced by sliding activation in cilia are, as Fig. 18 shows, about a factor of five smaller than those produced by the activation of the fibers over the entire length. In flagella the superposition of the two mechanisms would lead to a waving perturbation of the linearity and of the (ideally zero) phase of the total active moment. Close inspection of Fig. 4 of Rikmenspoel (1971) shows that these perturbations are indeed present in the linearity and the phase of the active moments of invertebrate sperm flagella.

The mechanisms in cilia found in the present paper and the proposal by Rikmenspoel (1971) on the mechanism in flagella are therefore compatible and mutually supportive. We cannot say, however, that this constitutes a proof for the proposed mechanism in flagella. Such a proof could probably only be found in a direct experimental demonstration of the activation of fibers over their entire length, such as occurs during the effective stroke in cilia. In flagellar fragments of bull spermatozoa such an experimental demonstration has recently been given (Rikmenspoel et al., 1973). Bull sperm flagella have a much more complicated morphology than invertebrate sperm flagella, however, and the validity of results cannot be directly transferred.

Other mechanisms for the coordination of sperm flagellar contractility have been proposed by Lubliner and Blum (1971, 1972) and by Brokaw (1972 *a*, *b*). Both have in common that the initiation of the dynein-tubulin interaction is caused by sliding of the filaments due to curvature of the flagellum. The moments thus produced are assumed to *increase* the curvature. In both models sliding is assumed to occur only where a change in curvature occurs. A change in curvature affects, however, sliding at all locations distal to it (compare Eq. 20). This, combined with the fact that in both models the moments produced by the dynein molecules are summed only over the adjacent curved section of the flagellum, means that the models could be more properly called "semilocal" ones.

In the models of Lubliner and Blum and of Brokaw, the induced contractility tends to continue to curl the flagellum, and limiting factors such as a time delay between curving and contractile activity, shear stresses, internal viscosity and nonlinear elasticity are introduced to prevent divergence. With these factors both models are successful in demonstrating the development of waves in flagella, and in explaining the change in the traveling velocity of these waves with external viscosity (Lubliner and Blum, 1972; Brokaw, 1972 *b*, *c*).

The mechanism proposed by Rikmenspoel also leads to the development of waves (Skalafuris and Rikmenspoel, 1973).[4] The dependency on viscosity of the traveling velocity of waves in sperm flagella can be explained with considerable accuracy from the ratio of the stiffness of the flagellum and the viscosity only (Rikmenspoel, 1971).

All three models are therefore equally successful in explaining wave properties. The models of Lubliner and Blum and of Brokaw both propose mechanisms for the contractile coordination in flagella which are at variance with those in cilia found in this paper. Until a direct experimental demonstration of the coordinating mechanism in flagella has been made, none of the three models discussed can be taken as confirmed, however.

We wish to thank Mrs. Jacqueline Seemann for her assistance with the writing and running of the computer programs.

This investigation was supported in part by the National Institute of Child Health and Human Development through grant HD-6445.

Received for publication 2 April 1973.

REFERENCES

AFZELIUS, B. A. 1959. *J. Biophys. Biochem. Cytol.* **5**:269.
AFZELIUS, B. A. 1961. *J. Biophys. Biochem. Cytol.* **9**:383.
BABA, S. A., and Y. HIRAMOTO. 1970. *J. Exp. Biol.* **52**:675.
BROKAW, C. J. 1972 *a*. *Biophys. J.* **12**:564.
BROKAW, C. J. 1972 *b*. *Science (Wash. D.C.)*. **178**:455.
BROKAW, C. J. 1972 *c*. *J. Mechanochem. Cell Mot.* **1**:151.
FAWCETT, D. W. 1966. The Cell. Its Organelles and Inclusions. W. B. Saunders Co., Philadelphia.
GIBBONS, I. R. 1963. *Proc. Natl. Acad. Sci. U. S. A.* **50**:1002.
GIBBONS, I. R., and E. FRONK. 1972. *J. Cell Biol.* **54**:365.
GOLDSTEIN, S. F. 1969. *J. Exp. Biol.* **51**:431.
GRAY, J., and G. J. HANCOCK. 1955. *J. Exp. Biol.* **32**:802.
HANCOCK, G. J. 1955. *Proc. R. Soc. Lond. A Math. Phys. Sci.* **217**:96.
HARRIS, J. E. 1961. *In* The Cell and the Organism. J. A. Ramsay and V. B. Wigglesworth, editors. Cambridge University Press, London.

[4] Brokaw (1972 *a*) has attempted to show that activation of the contractile fibers over their entire length would not lead to the development of waves. In Brokaw's calculation technique all moments are supposed to vanish at the base of the flagellum which is incompatible with a summing of moments towards the base. It is therefore a priori excluded that Brokaw's computation technique when applied to Rikmenspoel's proposal could lead to meaningful results.

HUXLEY, A. F. 1957. *Prog. Biophys. Biophys. Chem.* **7**:281.
KINOSITA, H., and A. MURAKAMI. 1967. *Physiol. Rev.* **47**:53.
LAMB, H. 1952. Hydrodynamics. Cambridge University Press, London. Sixth edition.
LUBLINER, J., and J. J. BLUM. 1971. *J. Theor. Biol.* **31**:1.
LUBLINER, J., and J. J. BLUM. 1972. *J. Theor. Biol.* **34**:515.
MILLER, P. L., editor. 1968. Aspects of Cell Motility. Symposium of the Society of Experimental Biology. Academic Press, Inc., New York. **22**.
RIKMENSPOEL, R. 1966. *Biophys. J.* **6**:471.
RIKMENSPOEL, R. 1971. *Biophys. J.* **11**:446.
RIKMENSPOEL, R., S. E. ORRIS, A. C. JACKLET, and C. B. LINDEMANN. 1973. *J. Mechanochem. Cell Mot.* In press.
RIKMENSPOEL, R., and W. G. RUDD. 1972. IV International Congress of Biophysics, Moscow. Abstract E VIII a517.
RIKMENSPOEL, R., and M. A. SLEIGH. 1970. *J. Theor. Biol.* **28**:81.
RIKMENSPOEL, R., and G. VAN HERPEN. 1969. *Biophys. J.* **9**:833.
SATIR, P. 1965. *J. Cell Biol.* **26**:805.
SATIR, P. 1968. *J. Cell Biol.* **39**:77.
SKALAFURIS, A. J., and R. RIKMENSPOEL. 1973. *Biophys. Soc. Annu. Meet. Abstr.* **13**:212a.
SLEIGH, M. A. 1962. The Biology of Cilia and Flagella. Pergamon Press, New York.
SLEIGH, M. A. 1968. *In* Aspects of Cell Motility. P. L. Miller, editor. Academic Press, Inc., New York.
SLEIGH, M. A., and M. JARMAN. 1973. *J. Mechanochem. Cell Mot.* In press.
SOMMERFELD, A. 1947. Vorlezungen über Theoretische Physik. Band II. Mechanik der Deformierbaren Medien. Dieterich'sche Verlagsbuchshandlung, Wiesbaden, Germany.
SUMMERS, K. E., and I. R. GIBBONS. 1971. *Proc. Natl. Acad. Sci. U. S. A.* **68**:3092.